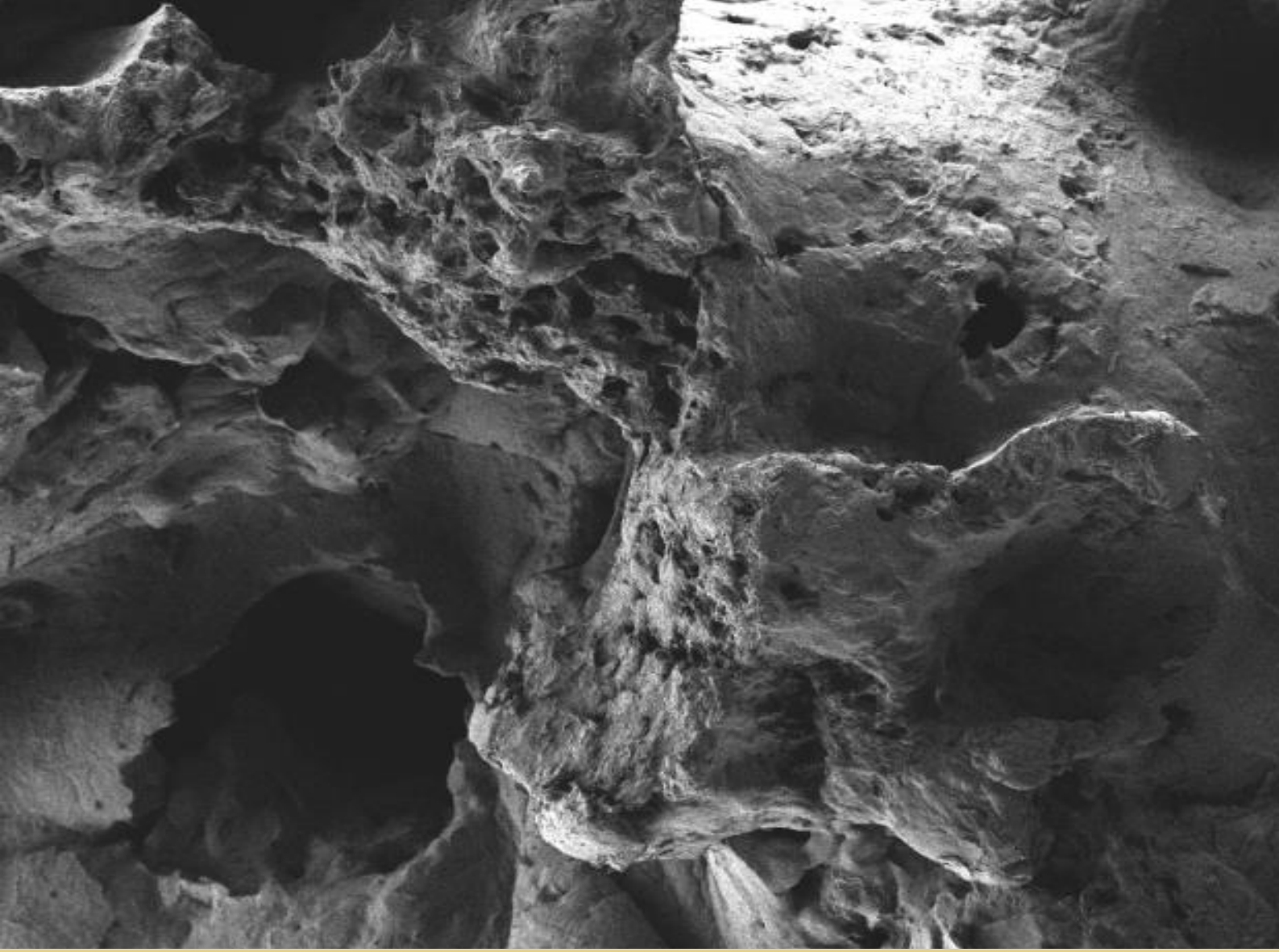

João André de Silveira Dias Gouveia

Green Methods for the Preparation of Novel Bone Cements Incorporating Highly Porous PCL/SBA-15 Composite Biomaterials

Master's Thesis in Biomedical Engineering
Presented to the Chemical Engineering Department of the Faculty of Sciences and Technology of University of Coimbra

February 2017

· U C ·

UNIVERSIDADE DE COIMBRA

• U C •

FCTUC FACULDADE DE CIÊNCIAS
E TECNOLOGIA
UNIVERSIDADE DE COIMBRA

João André de Silveira Dias Gouveia

Green Methods for the Preparation of Novel Bone Cements Incorporating Highly Porous PCL/SBA-15 Composite Biomaterials

Dissertation presented to University of Coimbra to obtain a Master's Degree in Biomedical Engineering

Supervisors:
Prof. Dr. Hermínio José Cipriano de Sousa (DEQ-UC)
Dra. Mara Elga Medeiros Braga (DEQ-UC)

Coimbra, 2017

This work was developed in collaboration with:

FCTUC

FCTUC FACULDADE DE CIÊNCIAS
E TECNOLOGIA
UNIVERSIDADE DE COIMBRA

Acknowledgements

This work was only possible with the precious help of my advisers, Professor Hermínio de Sousa and Professora Mara Braga. Thank you for all the availability.
I would like, also, to thank to Professora Ana Dias, Doutora Patrícia Coimbra, Rui, Luísa, Sofia, Akel and Rafael from our research group, and many thanks to Professor António Alberto for helping with the mechanical assays.
I would also like to thank to my family and to my friends that accompanied me during this stage.

Abstract

Bone cement is a biocompatible setting biomaterial used for bone defect fill that must have similar features to bone and dental tissues. Available calcium phosphate-based bone cements reveal high microporosity (enable deposition of biological molecules and nutrients/metabolic wastes flow) and have higher chemical similarities to bone calcium hydroxyapatite. However, they reveal low mechanical performance (to high load-bearing application areas) and low macroporosity (for osteoblast migration and consequent bone regeneration).

Different formulations of calcium phosphate/gelatine-based bone cements were produced incorporating highly porous pieces of poly(ε-caprolactone)/silica nanoparticles (92:8wt.%) (additivated with glycofurol, a porogenic, polymer/inorganic compatibilizer and plasticizer agent) processed by supercritical carbon dioxide-assisted foaming/mixing method. These biomaterials were produced in order to enhance morphological (such as surface area, macroporosity and bulk and real densities), mechanical (Young's modulus and compressive strength at break) and compatibility properties of the produced bone cements. The composition of pieces produced by supercritical foaming/mixing method to be incorporated into the calcium phosphate/gelatine-based bone cements was investigated. Morphological and mechanical properties of the produced bone cements were evaluated and hemocompatibility and osteogenic drug release (dexamethasone) assays were also performed.

It was concluded that the produced bone cements are fast-setting (~7.5 minutes). The higher weight percent composition of pieces (12 wt.%) produced by supercritical foaming/mixing method did not directly enhance the properties of the bone cements. However, some of the produced bone cements showed higher values of mechanical properties (such as 45 MPa and 2.1 MPa for Young's modulus and compressive strength at break, respectively) and porosity (>70%) (particularly, revealing high macroporosity) when compared to other commercial calcium phosphate cements (such as Ostim® and ChronOS®Inject). It was also concluded that the produced bone cements are able to release dexamethasone for an estimated period of 21 days, which is considered by the literature as a suitable time interval to stimulate bone regeneration.

It was concluded that the produced bone cements are candidates for bone/dental defect fillers, however more research should be performed to calcium phosphate cement

formulations, particularly on the weight percent composition of pieces produced by supercritical foaming/mixing method.

Keywords: composite biomaterials, hard tissue, poly(ε-caprolactone), SBA-15 mesoporous nanoparticles, supercritical carbon dioxide-assisted foaming/mixing, calcium phosphate/gelatine, fast-setting bone cements, dexamethasone release, bone defect

Resumo

Um cimento ósseo é um material biocompatível endurecível usado para preencher defeitos ósseos que deve possuir características parecidas com os tecidos ósseo e dentário. Os cimentos à base de fosfatos de cálcio disponíveis revelam alta microporosidade (permite a deposição de moléculas biológicas e o escoamento de nutrientes/lixos metabólicos) e têm "parecenças" químicas à hidroxiapatite de cálcio do osso. No entanto, revelam baixa eficiência mecânica (para aplicação em áreas de carga elevada) e baixa macroporosidade (para migração de osteoblastos e consequente regeneração óssea).

Diferentes formulações de cimentos à base de fosfato de cálcio/gelatina fora produzidos incorporando monólitos ralados muito porosos de poli(ε-caprolactona)/nanopartículas de sílica (92:8 % m/m) (aditivados com glicofurol, um agente porogénico, compatibilizante de polímero/inorgânico e plastificante) processados por uma técnica de foaming/mistura assistida por dióxido de carbono supercrítico. Estes biomateriais foram produzidos de maneira a melhorar as propriedades morfológicas (tais como área de superfície, macroporosidade e densidades aparente e real), mecânicas (módulo de Young e força de compressão à rutura) e de compatibilidade dos cimentos ósseos produzidos. A composição dos monólitos ralados produzidos pela técnica de foaming/mistura assistida por dióxido de carbono supercrítico a serem incorporados nos cimentos à base de fosfato de cálcio/gelatina foi investigada. As propriedades morfológicas e mecânicas dos cimentos ósseos produzidos foram avaliadas e ensaios de hemocompatibilidade e libertação de um fármaco osteogénico (dexametasona) foram realizados.

Foi concluído que os cimentos ósseos produzidos são rapidamente endurecíveis (~7,5 minutos). A alta composição mássica percentual dos monólitos ralados produzidos pelo método de foaming/mistura supercrítico (12 m/m %) não melhorou diretamente as propriedade dos cimentos ósseos. No entanto, alguns dos cimentos ósseos produzidos mostraram valores superiores de propriedades mecânicas (tais como 45 MPa e 2.1 MPa para o módulo de Young e força de compressão à rutura, respetivamente) e porosidade (>70%) (particularmente revelando alta macroporosidade) quando comparados com outos cimentos de fosfato de cálcio comerciais (tais como Ostim® e ChronOS®Inject). Foi também concluído que os cimentos ósseos produzidos são capazes de libertar

dexametasona até 21 dias, o que é considerado pela literatura como um intervalo de tempo adequado para estímulo da regeneração óssea.
Conclui-se que os cimentos ósseos produzidos são candidatos para enchimento de defeitos de osso/dentes, no entanto mais pesquisa deve ser realizada a formulações de cimentos de fosfato de cálcio, particularmente à percentagem de composição mássica dos monólitos ralados produzidos pelo método de foaming/mistura supercrítica.

Palavras-chave: biomateriais compósitos, tecido duro, poli(ε-caprolactona), nanopartículas mesoporosas SBA-15, foaming/mistura assistida por dióxido de carbono supercrítico, fosfato de cálcio/gelatina, cimentos ósseos rapidamente endurecíveis, libertação de dexametasona, defeito ósseo

List of Abbreviations and Symbols

Abbreviations

BET – Braunauer – Emmett – Teller method

BG – Bioglass

BJH – Barret – Joyner - Halenda method

CP – Calcium phosphate

CDHA – Calcium-deficient hydroxyapatite

CPC – Calcium phosphate cements

DCPH – dicalcium phosphate dihydrate

et al. – et alii, “and others”

FDA – Food and Drug Administration

GF – Glycofurol

HA – calcium hydroxyapatite

IUPAC – International Union of Pure and Applied Chemistry

L/P – Liquid-to-powder ratio volume

Milli-Q-water – Ultra pure water type 1

PCL – poly(ε-caprolactone)

PDS - poly(p-dioxanone)

PLLA – poly(L-lactic acid)

PTFE – poly(tetrafluoro ethylene)

SBA-15 – Santa Barbara Amorphous type 15

SDT – Simultaneous Differential Thermal Analysis

SEM – Scanning Electron Microscopy

SFM – Supercritical CO_2-assited foaming/mixing process

SNPs – silica nanoparticles

TCP – tricalcium phosphate

α-TCP – α-tricalcium phosphate

β-TCP – β-tricalcium phosphate

Symbols and Greek Letters

~ – Approximately

d – particle diameter

M_n – Number-average molecular weight ($g.mol^{-1}$)

Na_2HPO_4 – Sodium phosphate dibasic or sodium hydrogen phosphate

NaH_2PO_4 – Sodium phosphate monobasic

P – Pressure (MPa)

$scCO_2$ – Supercritical Carbon Dioxide

T – Temperature (ºC)

wt. % – weight percent composition (%)

ΔH_f – Enthalpy of fusion ($J.g^{-1}$)

$\Delta H_f^{\circ}(T_m^{\circ})$ – Enthalpy of fusion of the totally crystalline polymer ($J.g^{-1}$)

χ_c – Crystallinity Degree (%) (calculated by SDT)

List of Figures

Figure 8 – SEM photographs (2kVs) of the produced SFM-processed pieces in different magnifications: ×55 (A), ×184 (B) and ×8790 (C). Scale bar: 200µm; 100µm and 3µm, respectively.

Figure 9 - Total water mass loss along the time of the composite cements. Water was being lost since the cements were set to cure, at 37ºC. ●- G20N18P12 ●-G10N6P6 ●- G10N6P12 ●- G20N18P6 ●-G15N12P9 ●- G20N6P6 ●- G10N18P6 ●- G20N6P12 ●- G10N18P12.

Figure 10 – Digital photographs of cement produced composites (top and side view). Photographs are organized by gelatine content. Photographs of cements that appear with a hole inside are also representative of the duplicates. Scale bar: 1 cm.

Figure 11 - SEM photographs of representative parts of the produced cements with 10 and 15 wt. % of gelatine. The presented magnifications from top to down lines are 80×, 300× and 5000×, respectively. Scale bar from top to down: 1mm, 100µm and 6µm, respectively.

Figure 12 - SEM photographs of representative parts of the produced cements with 20 wt. % of gelatine. The presented magnifications from top to down lines are 80×, 300× and 5000×, respectively. Scale bar from top to down: 1mm, 100µm and 6µm, respectively.

Figure 13 – Inorganic/organic composition of all produced cements. Deviations are the difference between theoretical and obtained/real values of inorganic content on SDT.

Figure 14 – Mechanical performance of the composite cements: Young's Modulus, MPa, (A) and Compressive Strength, MPa (B).

Figure 15 – DXMT release profile with the cements that revealed the better mechanical performance along the first eight days of assay: DXMT/cement, mg/g released (A) and total Released DXMT, % (B).

List of Tables

Table of Contents

1. Introduction

1.1. Goals and motivation

The main objective of this work is to develop bone cement composite biomaterials for hard tissue defect fill by a green chemistry methodology. Specifically, it is proposed to produce highly porous composites based on poly(ε-caprolactone)/SBA-15 silica nanoparticles (PCL/SNPs) by Supercritical-CO_2 assisted Foaming/Mixing (SFM) method and to incorporate them into a calcium phosphate/gelatine-based bone cement, so that it develops an osteoconductive biomaterial able to be injected into bone defects. Other specific objective is to perform morphological and mechanical characterizations and hemocompatibility and drug release assays to the produced biomaterials.

Thus, PCL was used as a biocompatible and biodegradable polymer for SFM biomaterials production. SBA-15 silica nanoparticles, a mesoporous biocompatible inorganic widely used in SFM technology, was mixed with PCL (since polymers do not reveal enough mechanical and morphological properties to be applied alone in hard tissue engineering applications). It was also added glycofurol (GF), a porogenic, polymer/inorganic compatibilizer and plasticizer agent to the mixture. Composite monoliths (PCL+SBA-15+GF) processed by SFM were then grinded into smaller pieces to be incorporated into calcium phosphate/gelatine-based bone cements. Calcium phosphates are biocompatible inorganic biomaterials with similarities to the bone/dental tissue. Porcine gelatine was added to enhance biocompatibility, porosity and compressive strength at break of the produced cements. It was also added an accelerator to improve setting time and an osteogenic drug (dexamethasone) to conclude about cements release profile.

To the best of our knowledge, this is the first study where is performed an incorporation of biodegradable and biocompatible highly porous PCL/SNPs biomaterials processed by SFM, into a calcium phosphate/gelatine-based bone cement in order to enhance biocompatibility, degradability, mechanical and morphological properties (such as surface area, pore diameter, macroporosity and bulk and real densities).

1.2. Generic properties of hard tissue (bone/teeth) cements

Biomaterials have been used in hard tissue engineering applications in order to repair/reconstruct bone and teeth defects and they must fulfil some essential requirements. Bone cements are biocompatible setting biomaterials used for implant fixation in multiple orthopaedic and dental procedures (acting as a glue that holds the implant/prosthesis against the adjacent hard tissue), or as a bone/dental substitute/defect filler (Vaishya *et al.*, 2013; Takahashi *et al.*, 1999; Bohner, 2000; Chow and Takagi, 2001; Blom *et al.*, 2002; Liu *et al.*, 2005; Lewis, 2006; Weir and Xu, 2008; Ikawa *et al*., 2009; Zhang *et al.*, 2014; Zhang *et al.*, 2015). Bone fractures/defects have impact in patient's quality of life (Balmayor and Griensven, 2015, Lai *et al*., 2013; Vaishya *et al.*, 2013; Denaro *et al*., 2009; Duarte *et al.*, 2004). To treat this kind of trauma, there are several clinical approaches reported in literature: a conservative management (including analgesics, bed rest, braces and rehabilitation) (Vaishya *et al.*, 2013, Denaro *et al*., 2009; Duarte *et al.*, 2004), autologous grafts (widely used, however they need an invasive and long surgery since bone is harvested, for example, from patient's iliac crest, which reveals osteoconductive properties), homologous grafts (involve the risk of immunological response) (Zhang *et al.*, 2014; Balmayor and Griensven, 2015; Duarte *et al.*, 2004), or a surgery using a suitable injectable/hand-filled bone cement, which is ideal for bone fractures or defects (Vaishya *et al.*, 2013; Zhang *et al.*, 2014; Lai *et al*., 2013; Balmayor and Griensven, 2015; Dickman *et al*., 1992).

Bone cements must have similar features to hard tissue (bone and teeth), such as chemical composition (Zhang *et al*., 2014; Yang *et al*., 2001; Balmayor and Griensven, 2015; Duarte *et al.*, 2004; Dickman *et al*., 1992; Vaishya *et al.*, 2013, Denaro *et al*., 2009; Lai *et al*., 2013). Teeth are composed of an inorganic part of dentin, enamel, dental pulp and cementum, but also composed of an organic part of collagen fibres and proteins. The bone has also an organic component (fibres of type I collagen) and an inorganic content of calcium hydroxyapatite (HA, $Ca_{10}(PO_4)_6(OH)_2$), others proteins and salts (Zhang *et al*., 2014; Yang *et al*., 2001). The mechanical properties of bone cements must also be similar to those of the hard tissue (Zhang *et al*., 2014; Yang *et al*., 2001; Zuo *et al*., 2010). Human trabecular bone has a minimum compressive strength at break of 130 MPa (transversal direction) and a maximum of 180MPa (longitudinal direction), revealing a highly porous (total porosity of ~79%) and blood irrigated component (Renders *et al.*, 2007; Yang *et al*., 2001). Cortical bone has a minimum

Young's modulus of 3000 MPa (transverse direction) and a maximum of 30000 MPa (longitudinal direction), revealing a compact material (osteocytes responsible for bone matrix calcification and homeostasis, and osteoclasts for bone resorption and renovation). It was also reported that the Young's modulus of dry collagen and bone calcium HA were 6000 MPa and 80000 MPa, respectively (Yang *et al.*, 2001).

A bone cement should also not require a difficult processing neither release toxic substances. It must reveal micropores, to allow deposition of biological molecules and to enable nutrients and metabolic wastes flowing. Ideally, should also reveal a high surface area and mesopores/macropores presence to enable new bone tissue grow and cell adhesion (Zhang *et al.*, 2014; Zhang *et al.*, 2015; Zuo *et al*., 2010; Bandyopadhyay *et al.*, 2006).

It was reported that, according to IUPAC (International Union of Pure and Applied Chemistry), micropores are smaller than 2nm and that macropores are larger than 50nm (Zdravkov *et al.*, 2007). However, according to Zhang *et al.*, (2015) and Forouzandeh *et al.* (2013), in bone cements research community, micropores are defined as pores smaller than a few microns (μm) and macropores are defined as pores larger than 100μm.

The pre-cement should also be able of being injected before setting and harden *in vivo* at physiological temperature, and also act as a drug delivery vehicle, preferentially with a controlled release (over time and local) (Forouzandeh *et al.*, 2013; Tiwari *et al.*, 2012; Jain, 2008; Harrison, 2007). The material should also be biodegradable with a degradation rate compatible with new bone formation (Zhang *et al.*, 2014; Zhang *et al.*, 2015; Bandyopadhyay *et al.*, 2006; Groot, 1983; Rey, 1990; Ratner *et al.*, 2004; LeGeros, 2008; Bohner, 2010; Bose and Tarafder, 2012, Pietrzak, 2008; Palmer *et al.*, 2008).

There are different examples of commercially-available bone cements for different biomedical applications: calcium phosphate cements (CPCs) (bone/dental defect fillers), bioactive glasses-based cements (BGs) (apatite layer formation on its surface and their high mechanical performance enables them to be used as artificial bone) and poly(methylmethacrylate) (PMMA)-based cements (particularly used as light cured implant glues/resins in dental surgeries) (Lai *et al*, 2013; Vaishya *et al.*, 2013; Kokubo, 1991; Lewis, 2006; Pietrzak, 2008; Palmer *et al.*, 2008). Bone cements based on calcium phosphates will be studied on this work.

1.2.1. Calcium phosphate cements properties

Calcium phosphate cements (CPCs) have been attracting attention due to their excellent biological behaviour (biocompatibility and osteoconductivity), similarities with the inorganic part of the hard tissue (such as calcium HA) and huge number of micropores (pores smaller than few microns) (Zhang *et al.*, 2015) that are ideal for biological molecules deposition, nutrients flow and removal of toxic products from cell activity (Zhang *et al.*, 2014; Zhang *et al.*, 2015; Bandyopadhyay *et al.*, 2006; Zuo *et al.*, 2010; Espanol *et al.*, 2009). Micropores are left by evaporation after cement setting or due to spaces between granules (Zuo *et al.*, 2010; Zhang *et al.*, 2014; Espanol *et al.*, 2009). It was reported that CPCs are also able to load bioactive substances (such as Bone Morphogenetic Proteins (BMPs) and Vascular Endothelial Growth Factors (VEGFs)) and osteogenic drugs (such as dexamethasone (DXMT) (Forouzandeh *et al.*, 2013)) and release them in a suitable period of time compatible with new bone formation (approximately along a month) without large physiologic fluctuations (Forouzandeh *et al.*, 2013; Tiwari *et al.*, 2012; Jain, 2008; Harrison, 2007). One of the main advantages of CPCs use is that, since it hardens *in vivo* at physiological temperature (~37 ºC) after several minutes (5 - 10 minutes), it is possible for the surgeon to fill bone defects with complicate shapes (by syringe assisted or manually moulding) performing a fast and less invasive procedure which contribute to reduce patient's discomfort/pain during the surgery (Unuma and Matsushima, 2013; Vaishya *et al.*, 2013; Zuo *et al.*, 2010; Montufar *et al.* 2009).

On the other hand, it was reported some drawbacks of CPCs, such as lack of macropores/mesopores, that are important for fast new bone grow (namely, osteoblasts migration and bone tissue proliferation) and resorption, which consequently causes that biodegradation occurs by surface degradation (from the outside to the inside) by dissolution process (Lewis, 2006; Espanol *et al.*, 2009; Zhang *et al.*, 2015; Unuma and Matsushima, 2013). The mechanical performance of CPCs is also normally low (such as Young's modulus and compressive strength at break) to a high load-bearing application area (hip joint, for example) (Zuo *et al.*, 2010; Zhang *et al.*, 2015). Bohner and Baround (2005) also reported that CPCs reveal low injectability (which may be critical for surgical procedure, since the pre-setting cement may not be efficiently extruded trough the syringe), probably due to phase separation between the solid and the liquid components.

Morphological (bulk density, total porosity, pore size, pore connectivity) and mechanical properties (compression strength at break and Young's modulus) of seven commercial CPCs available as injectable biomaterials for use in orthopaedic trauma surgery were investigated *in vitro* (Table 1) (Van Lieshout *et al.*, 2011).

Table 1 - Morphological and mechanical properties of seven commercial CPCs available as injectable materials (adapted from Van Lieshout *et al.*, 2011).

CPC Name	Bulk density ($g.cm^{-3}$)	Total porosity (open + closed) (%)	Pore size (μm)	Pore connectivity ($1.cm^{-3}$)	Compression strength (MPa)	Young's modulus (MPa)
BoneSource®	1.78	1.80 (0.95+0.85)	33.4	~0	16.54	491
Calcibon®	1.71	0.81 (0.21+0.60)	41.6	~0	33.95	790
ChronOS®Inject	1.70	6.64 (2.94+3.70)	91.1	~0	0.81	54
Eurobone®	1.79	2.45 (1.20+1.25)	162.2	~0	15.30	481
HydroSet™	1.74	3.20 (0.50+2.70)	63.1	27.17	14.91	360
Norian SRS®	1.74	0.48 (0.23+0.25)	47.2	8.77	25.64	674
Ostim®	1.29	52.66 (52.25+0.41)	58.3	5.80	0.24	6

Cements were prepared using a custom-made Teflon mould. The total porosity refers to the open and closed porosity and the connectivity density refers to the number of interconnected pores per unit of volume. Bulk density was calculated by the ratio between weight and volume of each sample. Morphological properties were measured by micro-CT scanning and mechanical properties were determined following unconfined compression tests (Van Lieshout *et al.*, 2011).

1.2.2. Calcium phosphate cements – chemical reactions

Calcium phosphate cements (CPCs) have been widely used in clinical procedures for dental and orthopaedic grafts. It is reported in literature that more than one calcium phosphate (CP) powders are mixed with the aqueous phase to form the pre-setting cement (Unuma and Matsushima, 2013; Zuo *et al.*, 2010; Montufar *et al.* 2009).

On the next table (Table 2) it is possible to see a list of different reported calcium phosphates used on CPCs and their chemical formulas.

Tricalcium phosphates (TCPs) are the most used for injectable cements. There is an amorphous phase (ATCP) and three polymorphs (crystalline phases) (α, α' and β). α polymorph is influenced by ionic environment and is produced by heating the low temperature β polymorph. α and β phases are both biocompatible, however α is more soluble and converts to calcium-deficient hydroxyapatite (CDHA) faster, which makes

it a perfect candidate to be used in a fast setting biomaterial. α' type only exists at temperatures above 1400 ºC (Carrodeguas and Aza, 2011).

Table 2 - Different calcium phosphates used on CPCs, abbreviations and chemical formulas (adapted from: Unuma and Matsushima, 2013; Montufar *et al.*, 2009).

Calcium Phosphate	Abbreviation	Chemical formula
Monocalcium Phosphate	MCP	$Ca(H_2PO_4)_2$
Dicalcium Phosphate	DCP	$CaHPO_4$
Tricalcium phosphate	TCP	$Ca_3(PO_4)_2$
Amorphous tricalcium phosphate	ATCP	
Tetracalcium phosphate	TeTCP	$Ca_4(PO_4)_2O$
Octacalcium phosphate	OCP	$Ca_8H_2(PO_4)_6$
Calcium-deficient hydroxyapatite	CDHA	$Ca_9(HPO_4)(PO_4)_5OH$
Calcium hydroxyapatite	HA	$Ca_{10}(PO4)_6(OH)_2$

The following chemical reactions represent the setting of CPCs (Eq. (1), Eq. (2), Eq. (3)) (Unuma and Matsushima, 2013; Montufar *et al*., 2009; Zuo *et al.*, 2010; Zhang *et al.*, 2014, Santos *et al.*, 1999).

$$3(Ca_3(PO_4)_2\ (s) + 3\ H_2O\ (l) \rightarrow Ca_9(HPO_4)(PO_4)_5OH\ (s) \quad \text{(Eq. 1)}$$

$$2CaHPO_4\ (s) + 2Ca_4(PO_4)_2O\ (s) \rightarrow Ca_{10}(PO_4)_6(OH)_2\ (s) \quad \text{(Eq. 2)}$$

$$2Ca_3(PO_4)_2\ (s) + Ca_4(PO_4)_2O\ (s) + H_2O\ (l) \rightarrow Ca_{10}(PO_4)_6(OH)_2\ (s) \quad \text{(Eq. 3)}$$

The setting reaction of CPCs are dissolution-reprecipitation reactions of calcium phosphate components to produce calcium hydroxyapatite (HA, $Ca_{10}(PO_4)_6(OH)_2$). In the dissolution process, calcium and phosphate ions are released from the initial component and the solution becomes oversaturated with the ionic concentration reaching a critical value. The release of H^+ ions from the initial calcium phosphates (such as $CaHPO_4$) may possible contribute for the pH dropping, creating a slightly acid environment that helps the dissolution process. Surrounding the powder material occurs the nucleation of the new phase (responsible for the creation of micropores) that continuously keeps growing until the cement is completely set (Zhang *et al.*, 2014; Bohner, 2007; Dorozhkin, 2008; Chow, 2009).

It was reported that α-tricalcium phosphate (α-TCP, α-$Ca_3(PO_4)_2$) when mixed with the aqueous phase is able to form calcium deficient hydroxyapatite (CDHA,

$Ca_9(HPO_4)(PO_4)_5OH$), which is the product of the Eq.(1). Tetracalcium phosphate (TeTCP, $Ca_4(PO_4)_2O$) when mixed with calcium hydrogen phosphate (DCPD, $CaHPO_4{\cdot}(2H_2O)$) (Eq. (2) and TCP mixed with TeTCP (Eq.(3) are both able to form calcium HA (Chow, 2009; Unuma and Matsushima, 2013; Montufar *et al*., 2009; Zuo *et al.*, 2010; Zhang *et al.*, 2014, Santos *et al.*, 1999).

1.2.3. Calcium phosphate/polymer composite cements, growing factors and accelerators

Calcium phosphates, are not strong and biocompatibility enough to be used in bone cement applications, so the incorporation of a biocompatible and biodegradable polymer raises as an option to produce composite bone cements with enhanced properties (Montufar *et al*., 2010; Zuo *et al.*, 2010; Zhang *et al*., 2015; Zhang *et al*., 2014; Huang *et al*., 2008; Dubruel and Vlierberghe, 2014; Unuma and Matsushima, 2013; Bankoff *et al.*, 2012). Several calcium phosphate cements (CPCs) formulations were proposed in the literature using biocompatible polymers, such as bovine gelatine (Montufar *et al.*, 2010; Zuo *et al.*, 2010; Zhang *et al*., 2015; Huang *et al*., 2008; Dubruel and Vlierberghe, 2014; Unuma and Matsushima, 2013), chitosan (Costa-Pinto *et al*., 2011), hyaluronic acid (Zhang *et al*., 2014), syringe-foaming polymers (such as hydroxylpropyl methylcellulose) (Zhang *et al*., 2015), poly(L-lactic acid) (PLLA) and PCL (Zuo *et al.*, 2010).

Several α-TCP cement formulations were produced with the liquid component prepared by adding 1, 10, 15 and 20 wt.% of bovine gelatine, a biocompatible polymer with the hard tissue (gelatine is denatured collagen, which is the main protein of the extracellular matrix) enhancing, thus, new bone forming cells adhesion to the cement. Bovine gelatine was used as a multifunctional polymer to obtain fast-setting α-TCP/gelatine-based cements since it is well known for its foaming properties (for example in food and pharmaceutical industries). Its foaming capacity is explained by its amphiphilic character, which consequently makes it a surface active compound (surfactant-like behaviour). It was also reported that gelatine incorporation do not delay bone setting reactions, contributing for a low invasive surgical procedure (Montufar *et al..*, 2010, Bankoff *et al.*, 2012). It was proved that bovine gelatine provides higher compressive strength at break, enhancing the cement flexibility (tenser load support) and material improved deformation up to 3% in some reported cases (Montufar *et al*., 2010; Zuo *et*

al., 2010; Zhang *et al.*, 2015; Huang *et al.*, 2008; Dubruel and Vlierberghe, 2014; Unuma and Matsushima, 2013).

Zhang *et al.*, prepared an injectable macroporous CPC for hard tissue engineering, through a syringe-foaming method with a viscous hydrophilic polymer solution. Hydroxylpropyl methylcellulose was used as a porogenic polymer, which is able to foam CPCs due to the incorporation of air bubbles. The final material had a huge number of macropores and enhanced values of mechanical properties, such as Young's modulus and compressive strength at break, comparable to those of trabecular bone. *In vivo* studies (femoral sites of rabbits) were also performed in order to evaluate the cement biocompatibility. It was observed a fast osteoblasts invasion and the formation of new bone in implantation site. Other important features of this composite revealed in this study were the self-setting and cohesive properties without requiring toxic, expensive or complex additives. One advantage of this method when compared to add porogenic additives to ensure interconnectivity of pores is that this one does not compromise workability, biocompatibility or mechanical performance (Zhang *et al.*, 2015).

Another study concerning incorporation of biodegradable polymers into a commercially available CPC (Calcibon®: 61% α-TCP, 26% $CaHPO_4$, 10% $CaCO_3$ and 3% precipitated HA) for bone regeneration was performed. Thus, electrospun biodegradable ultrafine fibres were incorporated into the pre-setting Calcibon®. Three types of PCL fibres (single fibre diameters of 1.1μm, 1.4μm and 1.9μm) and one type of PLLA (poly(L-lactic acid)) fibre (single fibre diameter of 1.4μm) were prepared by electrospinning and then mixed with the pre-setting CPC at fibre weights of 1%, 3%, 5% and 7%. The compressive strength at break and the number of macropores of the prepared CPCs increased with nanofibres incorporation. Particularly, fibres diameter did not affect mechanical performance. However, mechanical properties were enhanced with the fibre weight content. It was also proved that through this incorporation method, nanofibres formed highly porous channel-like structures, and that after their degradation, inter-connective pores suitable for bone regeneration were produced (Zuo *et al.*, 2010).

Osteoconduction of bone cements can be improved by addition of growing factors, such as Bone Morphogenetic Proteins (BMP-2 and BMP-7) and Vascular Endothelial Growth Factors (VEGFs). BPM-2 is widely used to treatments of patients with compromised bone healing and critical defects. This one can be combined with a drug

delivery matrix that protects BMPs from degradation or premature release, delivering the drug locally in a controlled and predicted way (Tiwari *et al*., 2012; Balmayor and Griensven, 2015; Deol, 1997). It is also possible to incorporate antibiotics, anti-cancer and anti-inflammatory drugs and enzymes into calcium phosphate cements (Bose and Tarafder, 2012).

Calcium phosphate cements should be completely set in approximately 5 minutes at physiological temperature in order to guarantee a short time surgery (Unuma and Matsushima, 2013; Montufar *et al*., 2009). It was reported that, in some cases, calcium phosphate setting reactions are slow when it is not used an accelerator in the liquid component. Therefore, sodium phosphate dibasic (Na_2HPO_4) or sodium phosphate monobasic (NaH_2PO_4) were added to accelerate the setting reaction (faster production of calcium HA) without compromising biocompatibility. In some cases, the liquid component was prepared by adding 7 to 18 wt.% of Na_2HPO_4 (Montufar *et al*., 2010).

1.3. Composite porous biomaterials production by SFM process

Conventional methods for porous biomaterials production

Polymers have been widely used in several industries and their synthesis and processing have gained attention in the past years (Liu *et al*., 2008; Salgado *et al*., 2004; Nalawade *et al.*, 2006; De Matos *et al.*, 2013; Harrison, 2007). However, several traditional methods of polymer processing (such as fibre felt, fibre bonding, electrospinning, freeze drying, solvent casting, particulate leaching, melt-moulding and solid free-form techniques) (Nalawade *et al.*, 2006; Eckert *et al*., 1996; Sauceau *et al*., 2011; Burg et al., 2000; Harrison, 2007; Salgado *et al*., 2004; De Matos *et al.*, 2013; Churro *et al.*, 2016; Rosa, 2013) make use of environmentally hazardous compounds (since they use volatile organic solvents or/and chlorofluorocarbons (CFC)) and may need an additional removal process or harsh processing conditions (such as high temperature that may compromise the use of thermolabile species, such as osteogenic drugs) (Nalawade *et al.*, 2006; Sauceau *et al*., 2011; Burg *et al.*, 2000; Harrison, 2007; Salgado *et al*., 2004; De Matos *et al.*, 2013; Churro *et al.*, 2016).

Supercritical carbon dioxide-assisted foaming process (SFM)

Supercritical CO_2-assisted foaming/mixing process (SFM) arises as an environmentally safe alternative to the traditional methods (in research laboratory but also on the

industries) (Nalawade *et al.*, 2006; Sauceau *et al*., 2011; Liu *et al.*, 2008; Eckert *et al*., 1996; Champeau *et al.*, 2015; Jenkins et al., 2006; Collins *et al*., 2008; De Matos *et al.*, 2013; Churro *et al.*, 2016; Rosa, 2013). A supercritical fluid is a substance for which both temperature and pressure are above their critical values, revealing intermediate properties between those of liquids and gases (Eckert *et al*., 1996; Nalawade *et al.*, 2006; Champeau *et al.*, 2015 Sauceau *et al*., 2011; Jenkins et al., 2006; Collins *et al*., 2008; Braga *et al.*, 2011; Natu *et al*., 2008; Churro *et al.*, 2016; Mooney *et al.*, 1996; Bhamidipati *et al.*, 2013). Supercritical CO_2 is one of the most used supercritical fluids, since it is a cheap and green versatile solvent with attractive physical and chemical properties (non-toxic, non-flammable, chemically inert, and its supercritical temperature and pressure are easily reached: 31ºC and 7.38 MPa, respectively) and can be easily removed from the material by depressurization and eventually recovered, not contributing to the greenhouse effect (Bhamidipati *et al.*, 2013; Champeau *et al.*, 2015; Nalawade *et al.*, 2006; Sauceau *et al*., 2011; De Matos *et al.*, 2013; Churro *et al.*, 2016). Poly(α-esters), for example: poly(glycolic acid) (PGA), poly(lactic acid) (PLA), poly(lactic-co-glycolic acid) (PLGA), poly(L-lactic acid) (PLLA) and poly(ε-caprolactone) (PCL) have been widely processed by SFM and are generally used in hard tissue substitution applications (Liu *et al.*, 2008; Zuo *et al*., 2010; De Matos *et al.*, 2013; Churro *et al*., 2016; Salgado *et al.*, 2004; Xu *et al*., 2004). PCL, particularly, has revealed interesting properties for hard tissue applications. It is a nontoxic FDA (Food and Drug Administration) approved polymer (compatible with hard tissue and several drugs) presenting also a long period of bulk degradation (approximately 3 years) (Burg *et al*., 2000; Zuo *et al*., 2010; Liu *et al.*, 2008; Salgado *et al.*, 2004; Churro *et al.*, 2016; De Matos *et al*., 2013).

Supercritical CO_2 acts as a polymer plasticizer, since it lowers the glass transition and melting temperatures of the polymer, allowing to process temperature sensible bioactive species/drugs (Salerno *et al*., 2014; Champeau *et al*., 2015; Sauceau *et al*., 2011; Nalawade *et al.*, 2006; De Matos *et al*., 2013; Churro *et al.*, 2016). The polymer may be mixed with an inorganic component (since polymers do not have enough morphological and mechanical properties to be applied alone in hard tissue applications), such as mesoporous silica nanoparticles (for example, SBA-15 silica nanoparticles, that have been often used as a biocompatible inorganic filler, revealing high surface functionalization, high surface area, high pore size and volume and present a superior drug-load/release performance) (Champeau *et al.*, 2015; Sauceau *et al*., 2011;

Churro *et al.*, 2016) and/or other polymers, such as polydioxanones (PDS) (a bioabsorbable polymer with shape memory developed specially for wound closure sutures) (Boland *et al*., 2005; Middleton and Tipton, 2000; Novotny *et al.*, 2012) and/or poloxamines (PLX) (an osteogenic polymer) (De Matos *et al.*, 2014).

Green plasticiser and polymer/inorganic compatibilizer agents were proposed to be used in SFM process (simultaneously with sc-CO_2) such as glycofurol (GF) (Figure 1), that has attracted special attention since it is a green nontoxic biocompatible FDA approved hydrotrope (surfactant-like behavior) already used as injectable solvent in pharmaceutical applications. It is constituted by a hydrophobic "head" and a hydrophilic "chain" that enhances $scCO_2$ solubility on the polymer matrix and increases compatibility between the polymer and the inorganic filler, lowering the interfacial tension and promoting a good material dispersion (silica nanoparticles into PCL matrix, for example). Other safe and green SFM additives (solvents, polymer/inorganic compatibilizers, porogenic or plasticizers) were reported in the literature, such as acetone, glycerol, ethyls, isosorbide dimethyl ether, limonene and ionic liquids with controlled toxicity (Liu *et al.*, 2008; Salerno *et al.*, 2014; Duarte *et al*., 2012; Churro *et al.*, 2016).

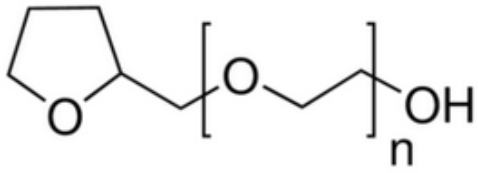

Figure 1 – Chemical structure of glycofurol (GF), the employed FDA approved plasticizer, porogenic and polymer/inorganic compatibilizer (supplier information).

Supercritical carbon dioxide-assisted foaming process (SFM) stages

The SFM processing is based on the high capacity of the polymer to absorb $scCO_2$ (Nalawade *et al.*, 2006; Sauceau *et al*., 2011; Champeau *et al.*, 2015; Liu *et al.*, 2008; Salerno *et al.*, 2014; Eckert *et al*., 1996; De Matos *et al.*, 2013; Churro *et al.*, 2016). In terms of processing, the SFM method can be described in three main steps. The first stage is characterized by a reduction of glass (T_g) and melting temperatures (T_m) ($scCO_2$ plasticizer effect) of the polymer (Salerno *et al*., 2014). Here, the polymer is soaked with $scCO_2$ and it is formed a solution of polymer/$scCO_2$. The viscosity and the

interfacial tension of the polymer is reduced. The second step is when it is obtained a homogeneous solution of the polymer and $scCO_2$. Reaching this equilibrium, the phase separation can be induced by causing a thermodynamic instability, such as a temperature rising or a pressure quench. On the second case, the instability causes the supersaturation of the dissolved CO_2 leading to bubble nucleation. The third step, is characterized by the nucleation and pore coalescence that was induced by the previously caused instability. The final growing/coalescence of pores due to the CO_2 concentration drop within the polymer creates the final tridimensional porous structure. The T_g of the polymer increases with the depressurization of CO_2, which leads to vitrification of the final structure (Bhamidipati *et al.*, 2013; Churro *et al.*, 2016; Eckert *et al*., 1996; Champeau *et al.*, 2015; De Matos *et al.*, 2013; Jenkins, 2007; Lee *et al*., 2011; Boland *et al*., 2005; Lu *et al*., 2013; Lanza *et al*., 2007).

2. Materials and Methods

2.1. Materials

Poly (ε-caprolactone) (PCL) (CAS [24980-41-4], density ~ 1.1 $g.cm^{-3}$), in pellet form, with a number average molecular weight (M_n) of 45,000 $g.mol^{-1}$, glycofurol (GF) (tetraglycol, CAS [31692-85-0], M_n = 190.24 $g.mol^{-1}$, density ~ 1.09 $g.cm^{-3}$ at 25 ºC), methanol HPLC (CAS [67-56-1], purity≥99.9%), acetone G.C. (CAS [67-64-1], purity≥99.5%), calcium phosphate (CP) (CAS [7758-87-4], purity≥96.0%, M_n = 310.18 $g.mol^{-1}$; density ~ 3.1 $g.cm^{-3}$), sodium phosphate dibasic dihydrate (Na_2HPO_4) (CAS [10028-24-7], purity≥99.0%, M_n = 177.99 $g.mol^{-1}$; density ~ 1.7 $g.cm^{-3}$), gelatine Type A from porcine skin with a gel strength of 300 (CAS [9000-70-8], M_n ~75,000$g.mol^{-1}$, density ~ 0.68 $g.cm^{-3}$) and dexamethasone (DXMT, purity ≥98.0%) were purchased from Sigma-Aldrich. PCL was mixed with inorganic SBA-15 silica nanoparticles. Two types of SBA-15 silica nanoparticles were used in different stages of this work (as it will be explained in section 2.2.2): Mesoporous silica 1D-Hexagonal SBA-15 type (average BJH (Barret, Joyner and Halenda method) framework pore size 8.5nm, BET (Brunauer, Emmet and Teller method) surface area 718 $m^2.g^{-1}$, total pore volume 0.93 $cm^3.g^{-1}$) was supplied by Claytec (USA); Silica, mesostructured SBA-15, 99% (porous silica, silicon dioxide, nanostructured silica) (CAS [7631-86-9]) was supplied by Sigma-Aldrich. Carbon dioxide (purity of 99.998% (v/v)) was supplied by Praxair (Spain). On this thesis, SBA-15 silica nanoparticles (both types) are, from this point forward, may be called as SNPs (silica nanoparticles) for an easier naming. Preliminary assays using thinner Bonelike® Spherical osteoconductive were also performed. These materials were gently supplied by Biosckin – Molecular & Cell Therapies S.A. Information about Bonelike® can be consulted on Appendixes A and B.

All the information about used materials was obtained from the suppliers and all materials were used as received except PCL, which was reduced from pellet into powder form (Appendix C).

The sterile rabbit blood (ACD-A 50 mL) used on the hemocompatibility assays was supplied by Probiológica – Empresa de Produtos Biológicos, Lda (Hemocompatibility assays were performed with the precious help of Luísa Filipe, Chemical Engineering Department, FCTUC).

2.2. Experimental Methods

In the figure 2, it is possible to observe a schematic representation of the experimental methods used in this work (flowsheet). SFM processed composite biomaterials were based on PCL (92 wt.% and 83 wt.%) and SBA-15 SNPs (8 wt. % and 17 wt.%).

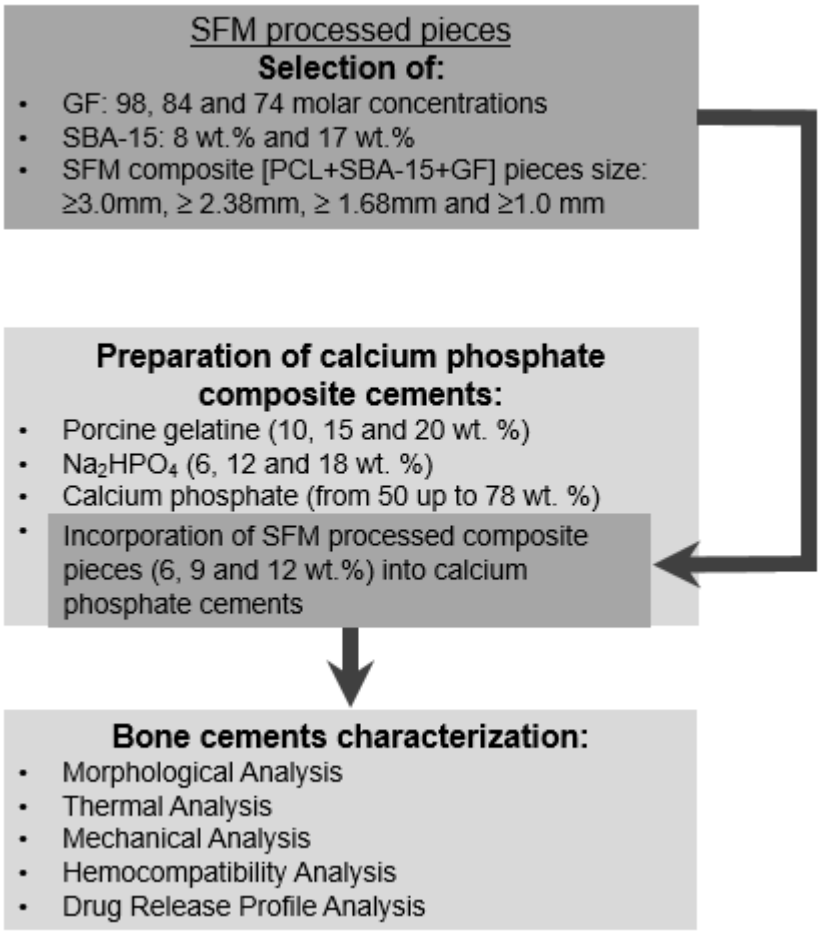

Figure 2 – Schematic representation of the experimental methods used in this work (flowsheet). SFM processed composite pieces were based on PCL(92 wt.% and 83 wt.%) and SBA-15 SNPs (8 wt. % and 17 wt.%). The weight percent composition (wt. %) is referred to the total cement formulation with exception to the SBA-15 weight percentage that is referred to the silica nanoparticles content (8 and 17 wt.%) of the SFM processed composite that will be incorporated into the cement.

The different formulations of calcium phosphate cements were produced as composite materials of porcine gelatine (10, 15 and 20 wt. %), Na_2HPO_4 (accelerator) (6, 12 and 18 wt.%), SFM processed composites (PCL + SBA-15 + GF) grinded pieces (6, 9 and 12 wt.%) (PCL particle size, SBA-15 wt.% and GF molar concentration were investigated before incorporation into calcium phosphate cements) and calcium phosphate (50 - 78 wt.%).

2.2.1. Preparation of calcium phosphate cements

To prepare 9 different cement formulations, calcium phosphate (50 - 78 wt. %), porcine gelatine (10, 15 and 20 wt. %), Na_2HPO_4 (6, 12 and 18 wt. %), SFM-processed composite pieces (6, 9 and 12 wt.%) and 7.5 mL of distilled water (0.5 mL each time) were physically mixed (Table 3). All the cements were produced in duplicate and by an aleatory order based on complete factorial design using the software JMP Pro 12.1.0 (SAS Institute Inc.). The composites G15N12P9 and G20N18P6 were also used to perform drug release profile assays (since they were the formulations that revealed higher mechanical performance, as it will be later explained). So, these composites were also mixed with dexamethasone (DXMT) (0.5 wt.%) on the preparation process.

Table 3 - Composite produced cements: abbreviations (cement sample column) and formulations.

Cement Sample*	**Calcium phosphate (wt. %)**	**Porcine gelatine (wt. %)**	**Na_2HPO_4 (wt.%)**	**SFM processed composite pieces (wt. %)**	**DXMT (wt. %)**
G10N6P6	78	10	6	6	0
G10N6P12	72	10	6	12	0
G10N18P6	66	10	18	6	0
G10N18P12	60	10	18	12	0
G15N12P9	64	15	12	9	0
G20N6P6	68	20	6	6	0
G20N6P12	62	20	6	12	0
G20N18P6	56	20	18	6	0
G20N18P12	50	20	18	12	0
G15N12P9 + DXMT	63.5	15	12	9	0.5
G20N18P6 + DXMT	55.5	20	18	6	0.5

***G: bovine gelatine; N:Na_2HPO_4; P: SFM processed composite pieces; DXMT: dexamethasone**

The relative content of each used chemical was based on the literature (Montufar *et al.*, 2010; Zuo *et al.*, 2010; Zhang *et al.*, 2015; Huang *et al.*, 2008). A porcine gelatine solution (10, 15 and 20 wt. %) at 25ºC was prepared and then mixed in an IKA® T18 basic Ultra-Turrax during 5 minutes, producing an emulsion. Next, the correspondent calcium phosphate powder was added and mixed for one minute. SFM-processed composite pieces were then added, and were mixed for one minute too. Na_2HPO_4 was then added to the mixture and mixed for 30 seconds. The total mixing time of all chemicals was about 7.5±0.5 minutes. Pre-setting cements were stored in aluminium

moulds and left for water evaporation at ~37ºC (Zuo *et al.*, 2010) until the mass of cements stabilized completely.

On the next section (2.2.2.) it will be explained how the SFM-processed composite pieces were prepared to be incorporated into the pre-cement.

2.2.2. Incorporation of SFM processed composite pieces into calcium phosphate cements

Before SFM process, PCL pellets were reduced to powder (decreasing the PCL particle size in order to enhance physical mixture, promoting its interaction with $scCO_2$ and reducing the needed processing/contact time (Rosa, 2013; Churro, 2015)). It was observed that a PCL powder with higher particle diameter was more difficult to mix with SBA-15 silica nanoparticles than powder with lower particle diameter. The preparation of PCL into powder form was optimized from previous works in order to minimize PCL waste. This process is explained on Appendix C. PCL powder and SBA-15 silica nanoparticles were physically mixed until homogenization of the mixture with the aid of a spatula, in a 5 mL polytetrafluoroethylene (PTFE) cylindrical beaker.

A good physical mixture is important particularly when PCL and SBA-15 have such a high bulk density difference (~ 1.1 $g.cm^{-3}$ and ~ 1.8 $g.cm^{-3}$, respectively, according to suppliers). Glycofurol (GF) was added in molar concentrations (GF, molar %) of 74, 84 and 98 to the PCL/SBA-15 (100:0; 83:17 w/w) (here, it was used SBA-15 from Claytec, also used in previous studies) (Rosa, 2013; Churro *et al.*, 2016). Composites of PCL/SBA-15 (92:8 % w/w) and GF in a molar concentration of 98 were also processed by SFM (here, it was used SBA-15 from Sigma-Aldrich). The SFM processed monoliths are listed on Table 3. All the samples were produced in duplicate. SFM produced monoliths were optimized for incorporation into the calcium phosphate cements. As it will be explained on the section 3, the composite A98 + 8% SNPs was the selected one.

SFM assays were performed with $scCO_2$ in the experimental apparatus of the Figure 3. The experimental apparatus, as well as the optimization of the operating conditions, were presented in previous works (Rosa, 2013; Churro *et al*., 2016). In the present work, all the samples were processed at pre-determined processing conditions, namely pressure of 20MPa, temperature of 40ºC, a soak/contact time of 2 hours and a depressurization rate of 0.3 $MPa.min^{-1}$ (~67 minutes).

Table 4 - SFM processed monoliths.

GF, molar % [1]	SFM PCL-based monoliths [2]	PCL particle size, wt. %			SBA-15 SNPs [3], wt.%
		d ≤ 0.250mm	0.250mm ≤ d ≤ 0.600mm	0.600mm ≤ d ≤ 1.000 mm	
74	A74	16.65	16.65	66.70	-
	M74	-	100	-	-
	T74	100	-	-	-
	A74+17%SNPs	16.65	16.65	66.70	17
84	A84	16.65	16.65	66.70	-
98	A98	16.65	16.65	66.70	-
	M98	-	100	-	-
	T98	100	-	-	-
	A98+17%SNPs	16.65	16.65	66.70	17
	A98+8%SNPs	16.65	16.65	66.70	8

[1] GF, molar %: glycofurol molar concentration (74, 84 or 98). Glycofurol density = 1.09 $g.cm^{-3}$ at 25ºC
[2] **A: all the three sizes of PCL powder; M: middle size of PCL powder; T: thinner size of PCL powder.**
[3] SNPs: SBA-15 silica nanoparticles.

The values of correspondent density and viscosity of $scCO_2$ were 839.8 $kg.m^{-3}$ and 7.8 × 10^5 Pa.s, respectively. These conditions were proposed for the production of porous biomaterials for hard tissue applications, considering the superior mechanical and morphological properties of the materials produced in previous works (Churro *et al.*, 2016; Bhamidipati *et al.*, 2013).

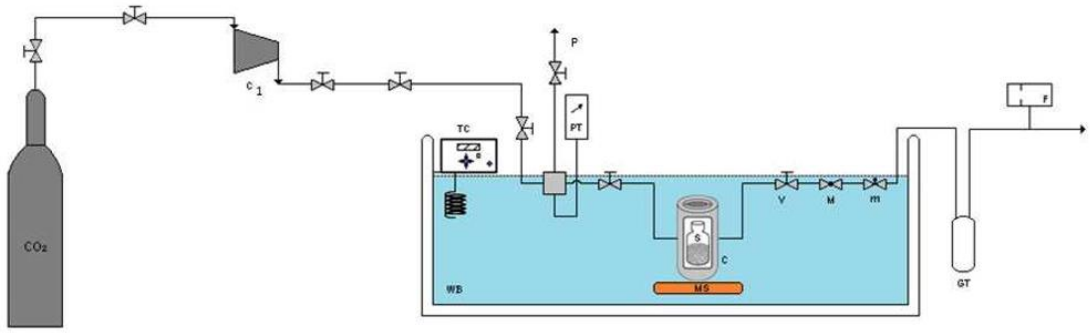

Figure 3 – Experimental apparatus for the $scCO_2$-assisted foaming/mixing process. CO_2 – carbon dioxide vessel; C_1 - compressor; TC – Temperature controller; WB – Water bath; P-purge; PT – pressure transducer; S – sample; MS – magnetic stirrer; C – High pressure vessel; V – Screw down valve; M – macrometric valve; m – micrometric valve; GT – glass trap; F – mass flow meter

Optimized SFM-processed composite monoliths of PCL/SBA-15 (92:8 % w/w) and GF (98 molar concentration), were grinded into smaller pieces in a 1000W Ariete Chopper Maxi, in 10±1 series of 3.0±0.5 seconds, avoiding PCL melting. They were then sieved using four test sieves with a width of ≥3.000mm, ≥2.380mm, ≥1.680mm and

≥1.000mm (Retshc 5657 Haan w., Germany). The pieces were then separated and weighed.

6, 9 and 12 wt. % of SFM grinded processed pieces, were physically mixed with the pre-setting cement, as described in section 2.2.1. The four sizes of processed pieces were incorporated proportionately according to the pieces size distribution after grinded: 8.78 wt.% of thicker pieces (2.380mm < d <3.000mm), 26.58 wt.% of pieces with 1.680 mm < d < 2.380 mm, 34.35 wt.% of pieces with 1.000 mm < d < 0.250 mm and 30.29 wt.% of thinner pieces (d < 1.000 mm).

2.2.3. Characterization Methods

Morphological Analysis

SFM processed samples and composite final cements were analysed morphologically.

Macroscopic analysis/observation was performed by visualization of digital photographs of SFM processed biomaterials and final cements taken with a resolution of 8 megapixels.

SFM pieces and cements were evaluated by SEM using a microscope (Jeol JSM-5310 Japan), with an operating voltage of 10kV. The samples were sputter-coated with gold for 10 seconds (approximately 5 nm thickness). Average pore diameter, on the range of approximately (50 – 450 μm) was determined by SEM image analysis (ImageJ® software).

For nitrogen adsorption and helium pycnometry all the samples were cut in 8 similar pieces, with a thickness inferior to 9 mm.

From nitrogen adsorption it was obtained the BET surface area (revealed a range of approximately (1.0 – 2.2 $m^2.g^{-1}$)), BET average pore diameter (revealed a range of approximately (3.8 – 18.0 nm)) and BJH pore volume (revealed a range of approximately (10 – 100 $cm^3.g^{-1} \times 10^4$)). Experiments were carried in an ASAP 2000 Micrometrics, model 20Q-34001-01.

From helium pycnometry it was obtained the real density (excludes void spaces inside the material). Experiments were carried in a Quanta-Chrome, MPY-2.

The bulk density was calculated indirectly by the ratio between the mass and the volume of the sample (which also includes the void spaces inside the material) (Unosson *et al.*, 2014; Bueno *et al*., 2016; Van Lieshout *et al*., 2011). The volume of the samples was

calculated considering that SFM biomaterials and final cements were approximately cylinders. It was used the formula:

$$V_{sample,}\, cm^3 = Base\ Area \times Height \quad \text{(Eq. 4)}$$

The values of total porosity, %, for all samples were also calculated indirectly by the formula (Bueno *et al.*, 2016; Barralet *et al.*, 2002; Unosson *et al.*, 2014):

$$Porosity,\ \% = 1 - \frac{Bulk\ Density}{Real\ Density} \quad \text{(Eq. 5)}$$

Thermal Analysis

Crystallinity degrees (PCL) χ_c (%), real inorganic contents (SBA-15 or calcium phosphate + Na_2HPO_4 + SBA-15) (wt.%), melting (T_m) (ºC) and thermal degradation (ºC) temperatures of SFM-processed biomaterials and cement formulations were evaluated on a simultaneous differential thermal analysis (SDT) equipment (Q600, TA Instruments). Approximately 8.5 mg of the produced materials were evaluated in a temperature range between 25ºC and 600ºC, at a 10 ºC min^{-1} heating scale. The crystallinity degree, χ_c (%), was determined by Equation 6 (Eq. 6), where $\Delta H_f(T_m)$ is the experimental melting enthalpy and $\Delta H^o_f(T^o_f)$ is the melting enthalpy of crystalline PCL (139.3 Jg^{-1}) (Churro *et al.*, 2016).

$$\chi_c\,,\% = \frac{100\Delta H_f(T_m)}{\Delta H^0_f(T^0_f)\left(1-\frac{SBA-15\ wt.\%}{100}\right)} \quad \text{(Eq. 6)}$$

Mechanical Analysis

The mechanical properties, compressive strength at break and Young's modulus at 2% strain, of the produced composite cements were determined using an oedometer (which was available on the Geotechnical Laboratory of Civil Engineering Department of FCTUC. Mechanical assays were performed with the precious help of Prof. António Alberto, Civil Engineering Department, FCTUC). The complete description of this analysis and sample preparation can be consulted in a previous work (Churro., 2015). Based on several studies, it was reported that mechanical tests to bone cements, namely calcium phosphate cements, were performed at a dry environment and at room

temperature (ISO 5833; ASTM E399; ASTM D790; ASTM C1341-00; Zuo *et al.*, 2010; Vallo *et al.*, 1998; Lidgren *et al.*, 1987).

Mechanical analysis was optimized from previous works since it was produced a suitable screw that perfectly fit the top of the sample, avoiding any movement while the compression test was performed, in order to guarantee more accurate results. Also, smaller loads were used at the beginning of the experiments to acquire more useful information. Therefore, the tests were performed by applying increasing loads, in each minute, of 0.005, 0.01, 0.03, 0.05 kg and conventional heavier loads, namely 0.250, 0.500, 1.000, 2.000 kg.

Hemocompatibility assays

Blood compatibility of the produced cements was studied performing direct (0.2g of cement sample per 1 ml of Drabkin modified solution) and indirect (7 ml of cement sample per 1 ml of Drabkin modified solution) contact assays. These studies were performed without (ASTM F 756, 2004) and with SBF immersion treatment for 72h, at 37ºC and 50 rpm (Kokubo *et al*., 2006; Sepulveda *et al.*, 2002). Assays were performed by using the cyanmethemoglobin method to quantify the haemoglobin (Hb) present in the blood (both erythrocytes and plasma haemoglobin) after the cements were in contact with the blood.

Drug release profile analysis

The two formulations with higher mechanical performance (G15N12P9 and G20N18P6) on the previous mechanical tests were selected in order to access their drug release profile (as seen in Table 3). Triplicates of each formulation were analysed by cutting 3 similar cylindrical slices of each. Cements were produced as explained in section 2.2.1. with the addition of 0.5 wt.% of DXMT (De Matos *et al.*, 2013) to the gelatine emulsion. They were involved in a dialysis membrane and their release profile assay was performed at 37ºC, without fluid renovation to evaluate the total DXMT released, using a spectrophotometer. The used standard curve for DXMT was $y=29.929x$ ($R^2 = 0.9951$) (for a wavelength of 242 nm).

3. Results and Discussion

All SFM biomaterials were processed under constant conditions and in a PTFE beaker that also avoid the formation of a non-porous coating. All the samples (SFM biomaterials and cements) were produced in duplicate, with exception to the cement samples produced to assess drug release profile, which were cut in triplicates after completely set. The presented results are the average and standard deviation of two (or three, for drug release profile) samples.

As explained previously on the flowsheet of this thesis (Figure 2), it was performed an incorporation of SFM-processed pieces into calcium phosphate/gelatine-based bone cements. The SFM processed biomaterials to be incorporated were produced as porous composite monoliths of PCL/SBA-15 (92:8 % w/w) and GF (98% molar concentration) and then grinded into smaller pieces. The wt.% of SBA-15 silica nanoparticles (from Sigma-Aldrich) was reduced from 17wt.% to 8wt.%, since with a larger weight percent composition did not stay homogeneously mixed with PCL at naked eye, which could be observed by the release of silica nanoparticles from the processed monoliths after SFM process. Despite GF could effectively work as porogenic agent (as it will be seen later in Figure 4) and polymer/inorganic compatibilizer agent when used in 74% molar concentration with SBA-15 from Claytec (as it will be explained on the section 3.1.1.), with this type of SBA-15 from Sigma-Aldrich it was necessary to use the maximum molar concentration of GF, 98 molar concentration, since with lower values of GF the silica nanoparticles were not homogeneously mixed with PCL.

On the section 3.1., it will be explained the selection of GF molar concentration and PCL particle size to produce SFM monoliths that will be, after this, grinded into pieces. Next, on the section 3.2., it will be discussed, particularly, the SFM processed pieces that resulted from the monolith grinding. Finally, on the section 3.3., the final formulations of calcium phosphate cements/gelatine (that will also include SFM pieces in their composition) will be discussed.

3.1. SFM monoliths: selection of GF molar concentration and PCL particle size

Assays for selection of GF molar concentration and of PCL particles size for SFM monoliths production were performed using one or three sizes of PCL powder previously sieved (small: $d < 0.250mm$; middle: $0.250mm < d < 0.600mm$ and thicker:

0.600mm < d < 1.000 mm) and then producing SFM PCL-based biomaterials, with 0, 8 or 17 wt. % of SBA-15 and with 74, 84 or 98 molar concentration of GF (Table 4). It was intended to use the three sizes of PCL powder to reduce waste (in previous works, only PCL particles middle size was used) and to reduce GF amount (in previous works only 98 molar concentration of GF was used), finding the minimum molar concentration value as it could work as porogenic, plasticizer and polymer/inorganic compatibilizer agent.

Considering that only two samples of each formulation were analysed and that the presented values were calculated by their average, it is understandable that, for several samples, the deviation value was substantial which is one of the main drawbacks of SFM, since the same materials produced under the same conditions stayed morphologically different (Churro *et al.*, 2016; Bhamidipati *et al.*, 2013).

3.1.1. Morphological Characterization

Macroscopic observation – The effect of PCL powder size, GF molar concentration and the content of SBA-15 silica nanoparticles were evaluated macroscopically. On Appendix D, it is shown the digital photographs of the obtained SFM monoliths and it is possible to observe their average values of diameter, height (Electronic Outside Micrometer), mass and volume after SFM process.

It is possible to produce PCL and PCL/SBA-15 (silica nanoparticles from Claytec) porous biomaterials using the three sizes of PCL powder. Particularly, it was observed that it was easily mixed with SBA-15 silica nanoparticles, since the processed composites were homogeneous at naked eye (which did not happen with other inorganic tested materials, namely Bonelike®) and it was not visible silica nanoparticles release from the material. Glycofurol acts as a polymer/inorganic compatibilizer agent helping the physical mixture between PCL and SBA-15 silica nanoparticles, as explained on the introduction of this work. In previous works, only 98 molar concentration of GF was used to guarantee a better polymer/inorganic mixture. So, in this work, it was investigated a minimization of the amount of GF on the PCL/SBA-15 composite, namely 84 and 74 molar concentrations. It was observed, macroscopically, that the composites stayed homogeneously mixed with dispersion of the silica nanoparticles within the PCL matrix, even with 74 molar concentration of GF**.** Comparing this information with Churro *et al.*, (2016) that also studied porous biomaterials with 98 molar concentration of GF, it is also visible here that the distribution of pore size is not

uniform: larger pores stayed on the bottom and the smaller pores stayed on the top of the sample (Appendix D) due to a lower CO_2 diffusion on the bottom during depressurization caused by a higher physical resistance. Pores seem to grow on the foaming direction (height direction), from bottom to top, since gas bubbles cannot coalesce freely on the radius direction. Bigger pores on the centre of the structure were possibly caused by heterogeneous distribution of GF. This global pore heterogeneity is a major disadvantage of this particular applied SFM process (since the used high-pressure vessel only had one exit for CO_2. It could be possible that, if the used vessel had more than one exit, probably the depressurization process would enable pore homogeneity of the sample) (Churro *et al.*, 2016; Rosa, 2013). However, for hard tissue engineering applications, this can be pointed out as an important feature, since it is required different pore size (micropores, mesopores and macropores, as already explained on the introduction of this work) (Zhang *et al.*, 2014; Zhang *et al.*, 2015; Bandyopadhyay *et al.*, 2006; Zuo *et al.*, 2010; Espanol *et al.*, 2009).

Generally, in this part of the work, by macroscopic visualization, it was observed that the three sizes of PCL can be used for SFM without significant variation on the macroscopic features and that GF works as polymer-inorganic compatibilizer agent with a minimum molar concentration of 74% since there was not silica nanoparticles release from the SFM monoliths.

All the results of nitrogen adsorption, helium pycnometry, bulk density and porosity (indirect calculations) are presented in the Table 5.

Nitrogen adsorption (BET surface area, BET average pore diameter and BJH pore volume) - The sample with higher surface area was the composite A74 + SNPs 17%. The incorporation of the inorganic filler promotes an increasing on the surface area due to a larger number of pores and a roughness surface (Sauceau *et al.*, 2011; Churro *et al.*, 2016; Rosa, 2013). A smaller amount of GF produces materials with higher surface of contact, which supports that GF can be used as a compatibilizer agent in 74 molar concentration instead of 98. The non-release of SBA-15 silica nanoparticles from the material also supports that GF can be used as a polymer/inorganic compatibilizer agent in 74 molar concentration.

The surface area is important for hard tissue engineering applications since it enables cell adhesion, proliferation and bulk biodegradation of the material (Harrison, 2007; Gautam *et al.*, 2013; Eckert *et al.*, 1996) that should be compatible with neobone

formation. Materials produced with 98 molar concentration of GF revealed, generically, reduced surface area (probably due to the formation of bigger pores) when compared to those produced with 74. Since 74 molar concentration (~9μL) is a much lower amount than 98 molar concentration (~133μL), it is possible that GF stayed more homogenously dispersed avoiding bigger accumulations on the centre of the sample, explaining the large discrepancy of values of surface area between samples produced with 74 and 98 GF molar concentration. Despite there was no reason found and its high value of deviation, the sample with lower surface area was the material produced with medium powder size and 98 molar concentration of GF, M98 (1.05±0.38 $m^2.g^{-1}$). An intermediate value of GF molar concentration (A84) was also tested in the optimization process, despite revealing a large deviation (1.29±0.38 $m^2.g^{-1}$). It was expected that the size of PCL particles did not influence the value of the surface area. The monoliths produced with three sizes, thin size or medium size, with 98 or 74 GF molar concentration did not present significant difference between them in terms of surface area, which supports the idea of using the three sizes proportionately to reduce PCL powder waste. The idea of using different PCL particle sizes was to help the initial physical mixture of SBA-15 silica nanoparticles with the polymer. It was also admitted that, independently of PCL particles size, all PCL was melted during SFM considering applied processing conditions, such as 2 hours of contact in a 40ºC bath, which is higher than PCL melting temperature in these processing conditions. Higher molar concentration of GF (98) produces pores with higher BET diameter. It was obtained porous monoliths with more than 100 Å of pore diameter with 98 molar concentration of GF, such as A98 (A = All sizes of PCL), M98 (M = Middle size of PCL particles) and A98+SNPs 17%. However, for the samples with three sizes of PCL and 74 molar concentration of GF (A74 and A74 + SNPs 17%), it was also obtained an average pore diameter higher than 100 Å, proving that the use of the three sizes of PCL particles (in order to help the silica nanoparticles dispersion within the polymer), instead of only one size, and 74 molar concentration of GF instead of 98 molar concentration, is perfectly acceptable to produce porous materials with this average pore diameter (despite all PCL is melted during SFM process).

The sample produced with thinner (T = Thinner size) PCL particles and with 98 molar concentration of GF (T98) revealed a value of average pore diameter much lower than the expected (42.30±5.53 $m^2.g^{-1}$) comparing with the other monoliths with 98 molar concentration. Inside of the groups of samples that were produced with 74 and 98 molar

concentration of GF, the samples that revealed higher BET average pore diameter also revealed higher BJH pore volume (A74, A74 + SNPs 17%, A98, M98, A98 + SNPs 17%) and vice-versa (M74, T74, T98 and also A98 + SNPs 8% pieces). The composite with 74 molar concentration of GF (A74 + SNPs 17%) has the higher value of pore volume (50.91±10.17 $cm^3.g^{-1}\times 10^4$) being even higher than the same composite (A98 +SNPs 17%) with 98 molar concentration (43.36±10.88 $cm^3.g^{-1}\times 10^4$). Despite the large deviations, it is possible to observe a trend that enhances the pore volume with lower GF molar concentration (74) and with 17wt.% of SBA-15 content.

Helium pycnometry (real density) - The samples produced with SBA-15 have higher values of real density (PCL real density ~ 1.1 $g.cm^{-3}$ and SBA-15 real density ~ 2.4 $g.cm^{-3}$) improving the real density of the composite when compared to the same formulation without silica nanoparticles. The GF molar concentration has almost no interference on the real density obtained values.

Bulk density - The indirect approach to calculate the bulk density (ratio mass/volume) of the samples arises as an alternative method of mercury intrusion (does not destroy the samples and it is a fast way, which does not depend on the availability of other equipment). However, as can be seen on Appendix D, samples produced through SFM process do not look exactly like a cylinder, mostly in the top of the sample, where it is possible to observe a mushroom-like rounded structure that interferes with assessment of samples height. This is an important disadvantage considering that the calculated value of bulk density through this method depends on the value of volume which directly depends on the value of height of the sample. That can explain the values of deviation between pairs of samples. However, laterally and on the bottom of the sample, it is possible to assume that melted PCL was moulded to the PTFE cylinder beaker. Bulk density refers to the density of the material considering volume occupied by the solid material and by void spaces inside. Generically, the presented values are lower when compared to previous works, which can probably be explained by the indirect applied method previously referred. However, it is interesting to observe that only two produced samples presented deviations higher than 0.04 $g.cm^{-3}$ (A98 and A98+SNPs 17%).

Table 5 - Obtained values from morphological characterization of the SFM-processed monoliths (A74, M74, T74, A74+SNPs 17%, A84, A98, M98, T98, A98+SNPs 17%) and pieces (A98+SNPs 8% pieces) biomaterials. It is also presented supplier information about SNPs.

GF [1], molar %	**SFM Biomaterials Based PCL**	**Nitrogen Adsorption**			**Helium Pycnometry**	**Indirect Calculation**	
		BET Surface Area, $m^2.g^{-1}$	BET Average Pore Diameter, Å	BJH Pore Volume, $cm^3.g^{-1} \times 10^4$	Real Density, $g.cm^{-3}$	Bulk Density, $g.cm^{-3}$	Porosity, %
74	A	1.38±0.17	104.09±65.34	33.2±18.12	1.11±0.01	0.28±0.03	74.48±0.03
	M	1.41±0.06	38.14±0.86	13.40±0.30	1.09±0.02	0.31±0.01	71.42±0.01
	T	1.50±0.01	40.29±2.31	15.15±0.85	1.11±0.00	0.32±0.03	71.07±0.02
	A+SNPs 17%	1.98±0.14	104.74±27.76	50.91±10.17	1.18±0.02	0.38±0.00	68.42±0.00
84	A	1.29±0.38	42.75±0.66	13.85±2.85	1.11±0.01	0.25±0.04	77.20±0.04
98	A	1.17±0.09	110.16±65.48	30.92±16.79	1.14±0.01	0.20±0.06	82.07±0.05
	M	1.05±0.38	160.57±115.03	31.15±14.81	1.12±0.01	0.23±0.02	79.07±0.02
	T	1.33±0.03	42.30±5.53	14.02±1.50	1.11±0.01	0.30±0.01	73.03±0.01
	A+SNPs 17%	1.14±0.29	152.59±0.35	43.36±10.88	1.19±0.01	0.31±0.05	72.71±0.04
	A+SNPs 8% pieces	**1.93±0.96**	**48.89±7.32**	**24.39±15.42**	**1.16±0.07**	**0.31±0.02**	**73.28±0.07**
SNPs (supplier) [2]		718	85	9300	~2.4	~1.8	~25*

GF[1] real density: 1.09 $g.cm^{-3}$

SNPs (supplier) [2]: Claytec SBA-15 silica nanoparticles. The presented information was obtained from supplier with exception of porosity (%)

* This porosity value for SNPs (%) was calculated by the indirect presented method.

A: all the three sizes of PCL powder; M: middle size of PCL powder; T: thinner size of PCL powder.

The sample with lower bulk density was the sample A98, and the sample A74+SNPs was the sample with higher bulk density. Monoliths with SBA-15 with 74 and 98 molar concentrations of GF (A74+SNPs 17%, A98+SNPs 17%) revealed the higher bulk density inside the group of samples produced with the same GF molar concentration (which is due to SBA-15 nanoparticles presence that have higher bulk density (~ 1.8 $g.cm^{-3}$) than PCL (~1.1 $g.cm^{-3}$)). It is clear that the addition of SBA-15 enhances the value of bulk density of the produced biomaterials.

Porosity - Considering the indirect calculated results for total porosity (Eq. 5) it is important to notice that the obtained values in this work are much higher than the presented results assessed by mercury intrusion by Churro *et al.*, (2016) for similar SFM porous monoliths processed under the same operating conditions. The values of porosity presented in this work directly depend on the values of the bulk density (also indirectly calculated), which present values much lower than the previous works. The values of porosity are higher for the samples produced with higher amount of GF (98 molar concentration) since it is effectively working as a porogenic agent improving the absorption of more CO_2 molecules within PCL chains by enhancing the solubility of the gas within the melted polymer (lowering interfacial tension of this mixture and the increasing of the nucleation rate). This effect is due to the polymer-compatible hydrophobic "head", since PCL and $scCO_2$ are both hydrophobic. On the contrary, it was stated that GF addition to similar SFM processed biomaterials was responsible for the formation of larger pores but with lower pore density, which yielded into materials with lower porosity (Champeau *et al.*, 2015; Sauceau *et al.*, 2011; Churro *et al.*, 2016; Rosa, 2013). On the group of samples produced with 74 molar concentration of GF, the sample with higher porosity was the sample produced with the three sizes of PCL powder (A74) (74.48±0.03%). This was also observed on the group of samples produced with 98 molar concentration of GF (A98) (82.07±0.05%). In Figure 4 it is possible to observe that the values of porosity are directly dependent on the values of GF molar concentration ($y=3.79x+70.32$, $R^2=0.97$). Generically, it is possible to conclude that GF works as porogenic agent, particularly when used on 98 molar concentration, however, it is also porogenic when used on 74 molar concentration (since the difference of porosity, %, between these two molar concentrations is less than 7%).

Obtained values of bulk density are higher for composite materials which revealed lower values of porosity, %. However, it was expected that the incorporation of SNPs led into an increase on the porosity value since they usually act as heterogeneous nucleation points (De Matos *et al.*, 2013; Rosa, 2013; Champeau *et al.*, 2015; Sauceau *et al.*, 2011; Churro *et al.*, 2016).

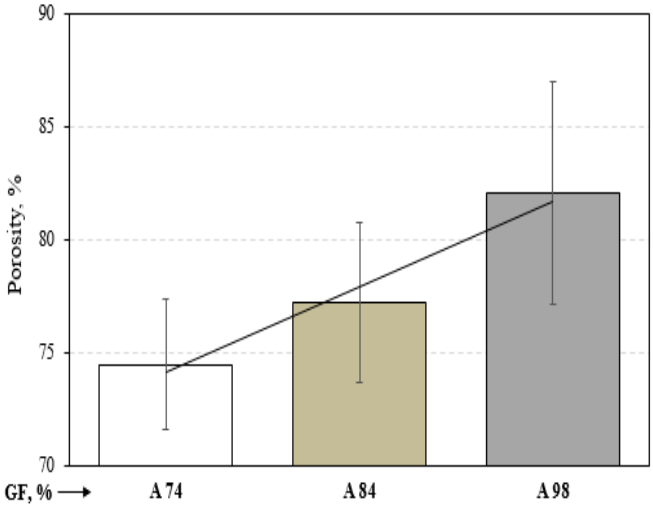

Figure 4 - Comparison of Porosity (%) of biomaterials produced with the three sizes of PCL powder and with 74, 84 or 98 molar concentration of GF (GF, %)

3.1.2. Simultaneous Differential Thermal Analysis (SDT)

Thermal analysis (SDT) was used to analyse the effect of GF molar concentration and silica nanoparticles presence on thermal and crystallinity properties of some of SFM-produced porous biomaterials. On the Figure 5, it is possible to observe the results of melting and degradation temperatures and degree of crystallinity (values can be consulted on Appendix E).

It is clear that melting temperature was not heavily influenced by GF molar concentration or silica nanoparticles presence, however, it is possible to see that composite biomaterials (with SNPs) produced with 74 (A74+SNPs17%) and 98 (A98+SNPs17%) molar concentrations of GF revealed slightly higher melting temperatures than the others materials (around 7%). It was expected, in order to verify GF plasticizer power, that the melting temperature of biomaterials produced with higher amounts of GF revealed a lower value (Salerno *et al.*, 2014; Churro *et al.*, 2016) however this was not observed in this work.

Observing the graphic B, it is clear that when the GF molar concentration is higher, particularly in presence of silica nanoparticles, the degradation temperature increased. This can be explained by a successful dispersion of the silica nanoparticles within the PCL matrix (GF polymer/inorganic compatibilizer action), leading to an increase of the thermal stability (and, consequently, a degradation temperature increase) possibility caused by the enhanced formation of "silica moieties" and PCL networks with higher GF molar concentration. It is possible to state that the degradation temperatures of the produced monoliths are much higher than physiologic temperature and they can be applied in hard tissue engineering biomaterials (Churro, 2015; Chen et al., 2012; Bonilla et al; 2014; Lee et al., 2005).

Considering crystallinity degree, the obtained values clearly show that PCL without SNPs and with lower GF molar concentration (A74) revealed the highest value (~86%). (The value of crystallinity degree of SFM processed pure PCL is around 70%) (Churro *et al*., 2016). It was reported that composite materials (PCL + SNPs) usually reveal lower crystallinity degrees, which can explain the higher value obtained for the non-composite material A74, particularly when compared to the same formulation with SNPs (A74+SNPs). It was reported that inorganic nanoparticles slow the crystallization of PCL, creating obstacles for the polymer chains to rearrange (since the free movement of the polymer chains is partially inhibited) which leads, consequently, to a lower value of crystallinity degree (Shieh *et al*., 2009, Churro *et al*., 2016). Crystallinity degrees of the other materials do not show high variation between them, since they are all near 40-60%. There was no explanation for these values.

From this first part of the work (3.1.), it was proved that GF acts as a polymer/inorganic (PCL/SBA-15 silica nanoparticles (Claytec)) compatibilizer agent when used in 74 molar concentration since there was not nanoparticles release from the SFM processed monolith. It was also observed that GF acts as porogenic agent when used in 74 molar concentration, and that the porosity of the materials are enhanced with GF molar concentration (Figure 4). Nitrogen adsorption values justified the use of the three sizes of PCL powder for production of SFM biomaterials, reducing material waste.

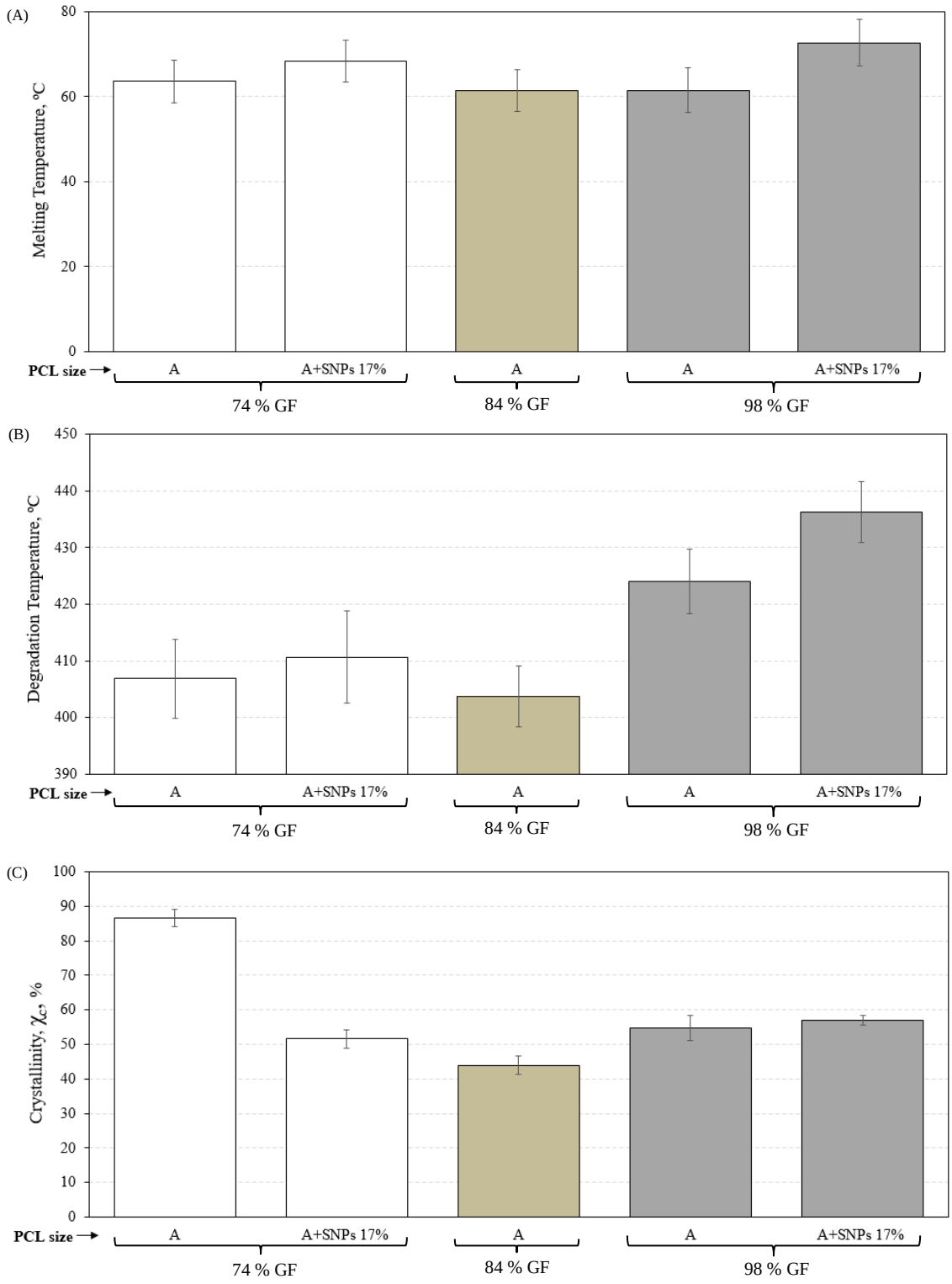

Figure 5 – Melting temperature (A), degradation temperature (B) and crystallinity degree, χ_c, (C) of the SFM processed biomaterials.

3.2. SFM-processed porous biomaterial pieces

3.2.1. Morphological Characterization

Macroscopic observation – In Figure 6 it is shown the digital photographs of the selected SFM monolith (PCL:SBA-15) (92:8) with 98 molar concentration of GF, before being grinded and sieved into pieces for cements incorporation. On the Table D.1. (Appendix D), it is possible to observe the average values of diameter, height (Electronic Outside Micrometer), mass and volume of the SFM monoliths that will be incorporated into calcium phosphate/gelatine-based bone cements.

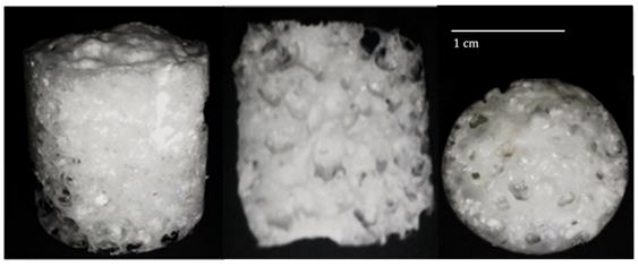

Figure 6- Digital photographs of a monolith of PCL:SBA-15 (92:8) with 98 molar concentration of GF (side, longitudinal cut and top view). All sizes of PCL powder were used. Scale bar: 1cm.

The samples prepared with 8 wt. % of SBA-15 silica nanoparticles are higher and, consequently, have more volume than samples prepared with 17 wt.% of silica nanoparticles from the fisrt part of this work (since the beaker was the same for all SFM biomaterials).

These SFM monoliths (PCL:SBA-15 (92:8) with 98 molar concentration) were then grinded into smaller pieces in order to be incorporated, proportionately according to the pieces size distribution after sieved, into calcium phosphate/gelatine-based cements. It is shown the digital photographs of the obtained pieces in the Figure 7.

The obtained values from nitrogen adsorption, helium pycnometry, bulk density and porosity of the SFM pieces can also be consulted on the Table 5 (A98+SNPs 8% pieces). The values of bulk density and porosity of the processed SFM pieces were assessed using the indirect method already explained.

Nitrogen adsorption (BET surface area, BET average pore diameter and BJH pore volume) - The value of surface area of the pieces (1.93±0.96 $m^2.g^{-1}$) is very close to the value obtained for the monolith A74 + SNPs 17% (1.98±0.14 $g.cm^{-3}$). SFM pieces revealed, generally, a high value of surface area when compared to the monoliths (with

exception to the A74+SNPs 17% monolith), which is an important feature for biomaterials to be applied in hard tissue engineering applications since it contributes to cell adhesion and new bone tissue grow (Zhang *et al.*, 2014; Zhang *et al.*, 2015; Zuo *et al*., 2010; Bandyopadhyay *et al.*, 2006). On the other hand, the obtained values for average pore diameter (48.89±7.32 Å) and pore volume (24.39±15.42 $cm^3.g^{-1}\times 10^4$) are relatively low when compared to the other produced materials, however, there was not found any explication for this. Nitrogen adsorption presented, for the produced pieces, pore diameters in the range of approximately (4.2 – 5.6) nm, which according to IUPAC, are considered mesopores, closer to the dimensions of micropores (< 2nm) (Zdravkov *et al.*, 2007). However, as previously explained in the introduction of this work, in bone cement applications, micropores are defined as pores smaller than a few microns (µm) and macropores are defined as pores larger than 100µm (Zhang *et al.*, 2015; Forouzandeh *et al.*, 2013), much higher values than the presented by nitrogen adsorption.

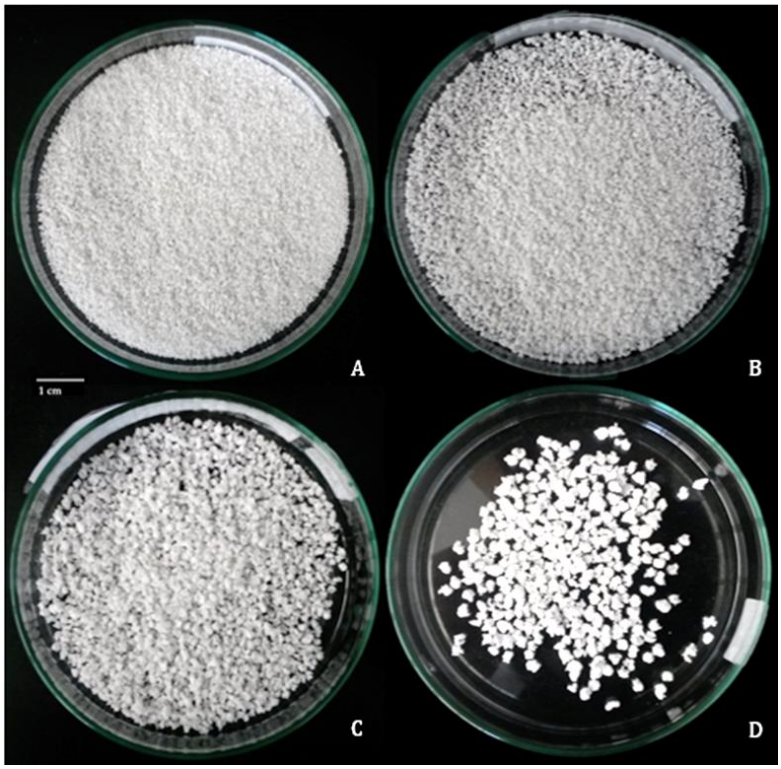

Figure 7 - Digital photographs of the four sizes of SFM pieces that were incorporated proportionately according to the particle size distribution after grinded and sieved: 30.29 wt.% of thinner pieces (d < 1.000 mm) (A); 34.35 wt.% of pieces with 1.000 mm < d < 0.250 mm (B); 26.58 wt.% of pieces with 1.680 mm < d < 2.380 mm (C) and 8.78 wt.% of thicker pieces (2.380mm < d <3.000mm) (D). Scale bar: 1cm.

Helium pycnometry - The value of real density (1.16±0.07 $g.cm^{-3}$) is between the values obtained for monoliths produced without (A98) and with 17% SNPs (A98 + SNPs 17%) (1.14±0.01 $g.cm^{-3}$ and 1.19±0.01 $g.cm^{-3}$, respectively), however SFM pieces reveal the lowest value of real density when compared to the other composites (A74+SNPs 17% and A98+SNPs 17%), which can be explained by the lower silica nanoparticles content (that have a real density of 2.4 $g.cm^{-3}$).

Bulk density and porosity - About the bulk density (0.31±0.02 $g.cm^{-3}$) and porosity (73.28±0.07 %) of the grinded pieces, it is possible to see that they are very close to the values of the composite A98+SNPs 17% (0.31±0.05 $g.cm^{-3}$ and 72.71±0.04 %).
The SFM pieces revealed to be highly porous biomaterials, it is also possible to see that they were the most porous composite produced biomaterial (comparing them with A74+SNPs 17% and A98+SNPs 17%).

Scanning Electron Microscopy (SEM) - SEM imaging was used to analyse the morphology of the produced SFM-processed pieces. In Figure 8, it is possible to observe different magnifications, namely ×55 (to observe, in a single image, the general morphology of one representative piece), ×184 (to observe the roughness of the surface) and ×8790 (where is possible to observe, probably, SBA-15 silica nanoparticles distribution on the PCL matrix). In Figure 8A, it is possible to see a global view of a SFM-piece with approximately 2.6 mm of diameter, revealing its irregular shape. Since these porous composite biomaterials were produced in order to be incorporated into calcium phosphate/gelatine-based cements and to "transfer" to them porosity and surface area, it is interesting to observe in the figure the existence of pores in the range of hundreds of micrometres. The average pore diameter were calculated for the processed pieces based on SEM imaging using ImageJ® software (as performed by Churro *et al.*, (2016) and Rosa (2013)). Concerning six evident irregular (not spherical) pores shown in the Figure 8A with red arrows, the calculated average pore diameter was 196.17±75.42 μm. The high value of deviation (~40%) represents the heterogeneous pore size of the SFM pieces. According to Zhang *et al.*, (2015) in hard tissue engineering applications, particularly concerning injectable bone cements for defect fill, pores larger than 100μm (macropores) are proper for bone regeneration since they facilitate osteoblast migration, cell adhesion and proliferation of the new-formed bone tissue, which would not be possible with smaller pores.

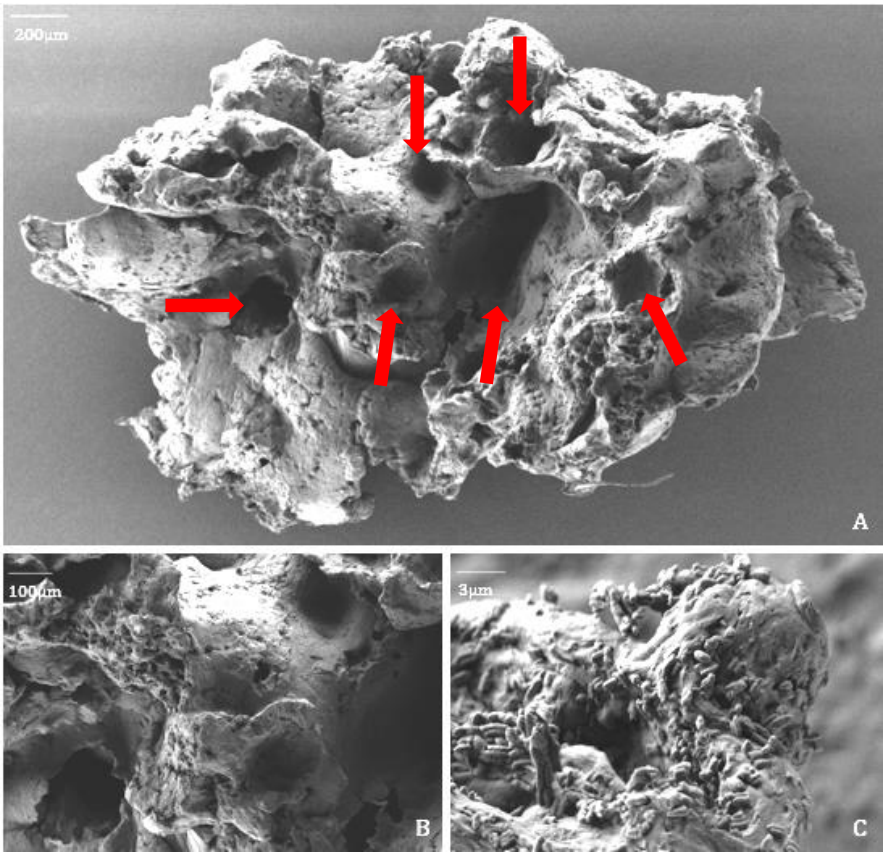

Figure 8 – SEM photographs (2kVs) of the produced SFM-processed pieces in different magnifications: ×55 (A), ×184 (B) and ×8790 (C). Scale bar: 200µm; 100µm and 3µm, respectively.

It was also stated in the literature that this value of pore size found on these pieces are in the range of values found for commercial CPCs, such as Eurobone®, that has an average of pore size of 162 µm or ChronOS®Inject, with an average pore size of 91 µm (Van Lieshout *et al.*, 2011). However, it will be necessary to perform the same calculation to final bone cements.

In Figure 8B, it is clear that these pieces are composed of a roughness surface, which appears to increase surface area (BET surface area values on the range of approximately (0.97 – 2.89) $m^2.g^{-1}$), ideal for hard tissue engineering applications, since it promotes adhesion of osteoblasts to the surface of the material (Cui *et al.*, 2015; Rosa *et al.*, 2013; Churro *et al.*, 2016).

In Figure 8C, it is visible some "bacillus" structures. It seemed that nanoparticles were homogeneously dispersed within PCL matrix. However, it is seen in this SEM image that silica appeared not to be homogeneously distributed in the polymeric matrix, probably because silica nanoparticles formed these agglomerated structures on the surface, however one single image might not be conclusive.

3.2.2. Simultaneous Differential Thermal analysis (SDT)

SFM-processed pieces were evaluated on a SDT equipment in a temperature range of 25 – 600 ºC (to guarantee that all PCL was completely degraded) in order to measure the effective percentage of weight of inorganic (silica nanoparticles). It was expected a value near 8 wt. % of inorganic content (effectively incorporated in the initial physical mixture). It was observed that the organic mass loss was 93.21±0.86 %, which consequently leads to a real SNPs content of 6.79±0.86 %. An example of the method for this calculation is presented on Appendix E.

Comparing the obtained value of inorganic content with the theoretical content, it presents a percentage deviation of 15.13%. This deviation could probably be caused by selecting non-representative pieces, since at naked eye it was difficult to choose pieces that were perfectly homogeneous in terms of PCL/SNPs mixture. Other explanation could be that some nanoparticles mass were lost in initial physical mixture with PCL. However, it was assumed that the obtained real inorganic content was close to theoretical value (8%). Thus, through SDT, it was concluded that SFM pieces were homogenously mixed.

3.3. Calcium phosphate bone cements

SFM-processed pieces were then incorporated into calcium phosphate/gelatine-based bone cements as explained in 2.2.1. Cements formulations were already presented in Table 3.

3.3.1. Morphological Characterization

Macroscopic observation – On the Appendix F, it is possible to observe the average values of liquid to powder ratio (L/P) volume, diameter, mechanical height (Electronic Outside Micrometer) (height normalization in order to perform the mechanical characterization with higher precision since mechanical height must be approximately 1.5 × diameter of each samples (Van Lieshout *et al.*, 2011)), mass and volume of the produced cements. Optimized mixing time of all chemicals, which was 7.5 ± 0.5 minutes as explained in 2.2.1., matched the setting time for some cases, making the moulding process difficult (into aluminium moulds). Since on the final seconds of the mixing time it was possible to observe setting granules of gelatine (independently of its

weight percentage) setting time was estimated to be on the interval of [0 - 1] minutes, behaving as a fast setting cement, despite not being possible to make a clear distinction between mixing and setting times. It was possible to find on the literature different definitions of bone cement setting time, such as based on the time at which a light/heavy Gillmore needle fails to make a perceptible circular indentation on the surface of the cement (ASTM C226, 2012) or the time interval in which the cement supported the maximum temperature (ASTM F451, 2008). In this work, the setting time was defined as the time interval that the liquid paste took to become not-liquid (Montufar *et al.*, 2010; Unuma and Matsushima, 2013). α-TCP-based cements have normal setting times of 5 – 10 minutes (Montufar *et al.*, 2010; Unuma and Matsushima, 2013; Zuo *et al.*, 2010). Thus, the produced cements in this work can be defined as fast-setting, however further characterization should be performed in order to evaluate "how fast-setting" they are.

The fast setting behaviour of the produced bone cements may be explained by the chemical interactions between their components. It was already explained that Na_2HPO_4 works as an accelerator, added to formulations in order to produce a bone cement with suitable time of setting compatible with surgeon manipulation and a low invasive surgery. The used porcine gelatine contributes to the dissolution reaction of the initial calcium phosphate. It was reported that gelatine may be adsorbed on the inorganic crystals of the calcium-deficient hydroxyapatite due to gelatine slightly acid behaviour, helping the dissolution reaction. Gelatine provides its charged groups (amines) as nucleation sites for the precipitating hydroxyapatite crystals accelerating their growth and nucleation (Boanini *et al.*, 2010). One of the main objectives of produce composite (inorganic + organic) cements is that it is possible to take advantage of the organic segment to provide flexibility and to add bioactivity through the inorganic content (Kokubo *et al.*, 2003). It was also reported a study where was produced PCL/gelatine composite nanofibrous porous biomaterials for bone regeneration. The physicochemical interaction between them was explained by hydrogen bonds between ester group of PCL and amine group of gelatine molecules (Gautam *et al*., 2013).

In Figure 9, it is presented cements total water mass loss (during evaporation time) at 37ºC.

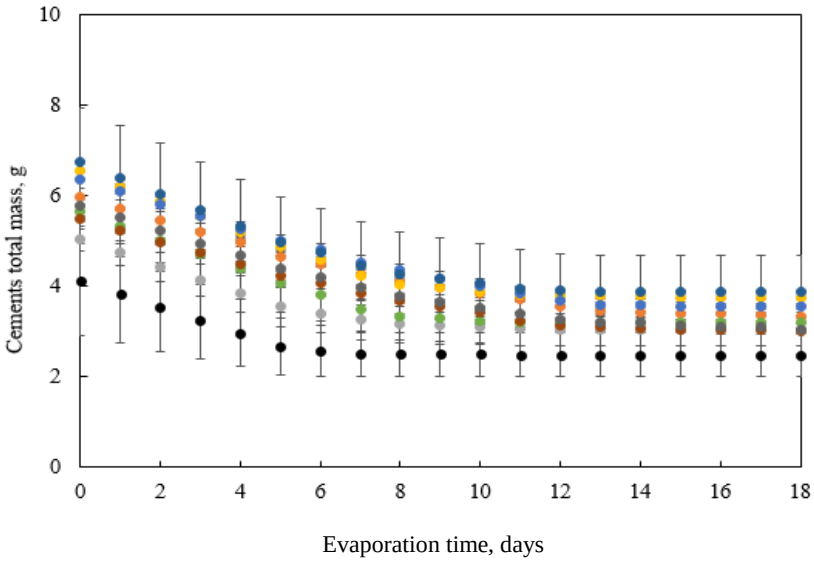

Figure 9 - Total water mass loss along the time of the composite cements. Water was being lost since the cements were set at 37ºC. ●- G20N18P12 ●-G10N6P6 ●-G10N6P12 ●- G20N18P6 ●-G15N12P9 ●- G20N6P6 ●- G10N18P6 ●- G20N6P12 ●- G10N18P12.

The total water evaporation time for these samples was around 12 days and it was the time necessary for the cement mass to stabilize (Zhang *et al.*, 2015; Zuo *et al.*, 2010), since from this point forward there was no more water loss (it was completely evaporated). The calculated average value of water loss was 52.7±2.5%, meaning that there was no large deviations between duplicated cement formulations. Furthermore, cements lost about half of their initial mass by water evaporation, since all the cements were produced with higher L/P ratios (~ 1) than those found on the literature for α-TCP cements (Montufar *et al.*, 2010; dos Santos *et al.*, 1999; Zhang *et al.*, 2015; Zuo *et al.*, 2010), which was necessary to perform a better gelatine emulsion and, consequently, a good physical mixture with the employed calcium phosphate. It is also shown the digital photographs of the produced composite cements, in Figure 10. It is clear that all the cements are approximately cylinders, since all of them were produced in a cylindrical aluminum mold. At naked eye, it is also visible that G10N6P12 and G20N6P6 have a big hole inside (happened to both duplicates) which was caused by a fast-setting reaction of the gelatine emulsion when mixed with the accelerator (despite these formulations were produced with the lowest content of accelerator, 6 wt.%) that adhere to the wall of the mold, not enabling that the liquid pre-setting cement paste reached the base. By macroscopic observation, it seemed that gelatine, calcium phosphate and

accelerant were homogeneously mixed, since there was no visible phase separation, which was guaranteed by a soft mixture of all used chemicals with the aid of a Turrax, as already explained. However, it was visible the incorporation of the SFM-processed pieces with different sizes on the top of the composite cements.

The values of bulk density and porosity of the produced cements were, once again, assessed using the indirect method already explained. All the morphological characterization of the produced cements is presented in the Table 6.

Nitrogen adsorption (BET Surface area, BET average pore diameter, BJH pore volume) - Contrary to expectations (Zuo *et al.*, 2010), the highest weight percentage of processed pieces (P) did not increase surface area. In fact, when added on 12 wt.% the values are generally lower than for 6wt. % of pieces, for similar formulations with the same weight percentage of accelerant (N) and gelatine (G). In future studies, it could be a good idea to increase SFM pieces wt. % up to 20 or 25 wt.% and to study their influence on the produced biomaterials when applied in higher content. However, the higher the weight percentage of Na_2HPO_4 (N), the higher the surface area is. Singly, the weight percentage of gelatine had no direct relation with the values obtained for surface area. However, the formulations with higher amounts of gelatine and accelerant (G20N18P6 and G20N18P12) revealed, synergistically, the highest values of surface area (2.16±0.70 $m^2.g^{-1}$ and 1.67±0.37 $m^2.g^{-1}$, respectively). The values obtained for BET average pore diameter do not reveal high variation between them (128.31±75.17 Å to 179.48±35.52 Å), however it was not possible to establish a relation between these values and cement formulations. The values obtained for pore volume have also low variation between them in general and there was not found any relation between cements formulations and pore volume. For some cases, it was visible that formulations with higher pore volume revealed higher BET surface area (G20N18P6, G20N18P12, G15N12P9 and G10N18P6) and vice-versa (G20N6P12, G20N6P6, G10N6P12).

Helium pycnometry - The used chemicals in the composite formulations have different values of density. Calcium phosphate, gelatine, Na_2HPO_4 and SFM processed pieces revealed values of real density of 3.14 $g.cm^{-3}$, 0.68 $g.cm^{-3}$, 1.7 $g.cm^{-3}$ and 1.16 $g.cm^{-3}$, respectively (supplier information or calculated value for SFM pieces by helium pycnometry). It was not found any general relation between the densities of these

materials and their weight percentage in the formulations with the obtained values of real density by helium pycnometry, since the presented values have no higher variation. Still, it is visible that the formulations G10N6P12 and G10N6P6 revealed the higher values of real density, which can be due to the high weight percentage of calcium phosphate, 78 wt. % and 72 wt. %, respectively.

Bulk density and porosity - The values obtained for bulk density were calculated indirectly by the ratio between the mass and the volume of each cement cylinder. The formulation (G10N6P6) with lower bulk density (0.28±0.04 $g.cm^{-3}$) and with highest porosity (87.46±0.36%) was the formulation produced with higher amount of calcium phosphate (78 wt. %). It was also reported in the literature that calcium phosphate can become porous after setting (Montufar *et al.,* 2009). In the other hand, the lowest value of porosity (71.73±10.20%) was for the formulation (G20N18P6) with only 56 wt.% of TCP, which also agrees with the previous result.

However, and contrary to expectations (Zuo *et al*, 2010; Zhang *et al*., 2015), the incorporation of SFM pieces did not have a direct impact on enhancing the values of porosity of the composite cements and neither the content of gelatine had (Montufar *et al.,* 2009; Zhang *et al.*, 2014), which also was expected, since it normally works as a porogenic polymer.

The values of bulk density of the produced cements are much lower (< 0.54 $g.cm^{-3}$) than commercially available CPCs bone substitutes, such as BoneSource®, Calcibon®, ChronOS®Inject, Eurobone®, Hydroset™, Norian SRS® that reveal bulk density values of approximately 1.75 $g.cm^{-3}$ (Table 1) (Van Lieshout *et al*., 2011). As already explained in this thesis it is known that biomaterials for hard tissue engineering applications must be highly porous. The presented cements reveal values of porosity much higher than other CPCs, namely, Ostim® that reveals a value of porosity of 53% (Van Lieshout *et al*., 2010), and (for some produced cements) even higher than the trabecular bone, that reveals a global porosity of 79.3% (Renders *et al.*, 2007).

Figure 10 – Digital photographs of cement produced composites (top and side view). Photographs are organized by gelatine content. Photographs of cements that appear with a hole inside are also representative of the duplicates. Scale bar: 1 cm

Scanning Electron Microscopy (SEM) – SEM imaging was used to analyse the morphology of the produced cements. In Figures 11 and 12, it is possible to observe different presented magnifications, namely ×80 (to observe, in a single image, the general morphology of one representative part of each cement), ×300 (to observe pore morphology and the roughness of the surface), ×5000 (for some detailed images). In Figure 11 it is possible to see cements produced with gelatine: 10 wt. % (1-4th column) and 15 wt. % (5th column). Cements produced with 20 wt. % of gelatine are presented in Figure 12.

By observation of the images with ×80 of magnification (first row of Figures 11 and 12), it is clear that all cements presented highly porous coral-like structures with tens of pores. The average pore diameter for the produced cements were calculated using ImageJ® software by analysing images with ×80 and ×300 of magnifications. The obtained values are presented on Table 6.

It appears that gelatine enhances pore diameter (producing bigger pores) in lowers concentrations than 20 wt.%, since all cements produced with this concentration revealed a lower average pore diameter than some cements prepared with 10 and 15 wt. %. On the other hand, the cement G20N18P12 is the material with lower average pore diameter and also with the lower deviation, which is clear by image observation, since all the presented pores are very similar in terms of size. It is also interesting to select the composite cement with higher heterogeneity considering pore size, which is the cement G20N18P6, presenting the higher deviation value. All the produced cements reveal high values of pore diameter deviation (~50% in some cases), which can be seen as an advantage for a bone cement.

As explained before, it was found in the literature average values of pore size of injectable commercial CPCs, such as 162 μm for Eurobone® and 91 μm for ChronOS®Inject (Van Lieshout *et al.*, 2011). Observing Table 6, it is clear that only one of the produced cements (G20N18P12) have lower value than Eurobone®. Generally, the materials with higher average pore diameter are cements G15N12P9, followed by G10N6P12 and then G10N6P6. All the produced cements revealed to be suitable candidates for hard tissue engineering applications in terms of morphology, namely for bone defect fill, since they are in the suitable range for these type of application with macropores in the range of 300-350μm (with exception to cements G20N18P12 and G20N6P6), which are proper for new bone tissue ingrowth. Mesopores (tens of micrometres) are also present, which induce biodegradation (namely bulk degradation), effective loading and release of bioactive compounds (such as osteogenic drugs) and good diffusion of blood and other body fluids throughout the porous material. In all cements, it is visible surface roughness, particularly in images taken at ×5000, which is probably caused by the setting of gelatine granules or the presence of smaller SFM-processed pieces, however, there was no evident relation between average pore diameter and weight percentage of pieces incorporation. This roughness increases the area of contact of the biomaterial, allowing better osteoblasts adhesion and, consequently, proliferation. In some cases, it is also possible to observe pores that appear to communicate (pore interconnectivity), namely in cements produced with 20 wt. % of gelatine, however additional studies should be performed to conclude about pore interconnectivity (Zhang *et al.*, 2015; Van Lieshout *et al.*, 2011; Zuo *et al.*, 2010).

3.3.2. Simultaneous Differential Thermal analysis (SDT)

The produced cements were evaluated on a SDT equipment in a temperature range between 25ºC and 600ºC (to guarantee that all the organic content, gelatine and PCL in this case, was completely degraded) in order to measure the effective percentage of weight of inorganic (calcium phosphate, Na_2HPO_4 and SNPs). In Figure 13, it is possible to compare the theoretical value of inorganic content with the real content per cement through the analyses of the deviation bar.

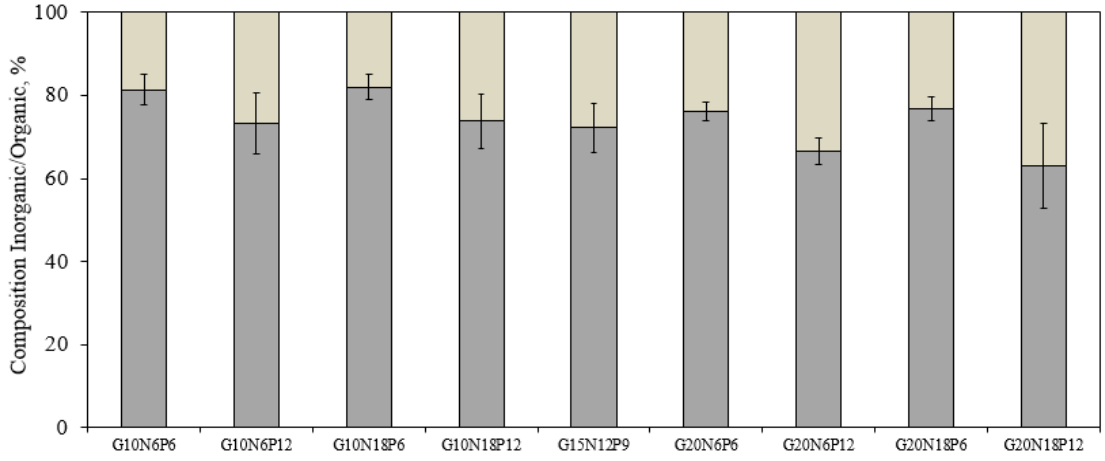

Figure 13 – Inorganic/organic composition of all produced cements. Deviations are the difference between theoretical and obtained/real values of inorganic content on SDT. ■ - inorganic content (wt. %) ■ – organic content (wt. %).

The composite formulation with higher deviation is G20N18P12 (~10%). Despite there was no general evidence considering the other values, it is possible to observe that this formulation was produced with lower inorganic content. All the other formulations reveal values of deviation lower than 7.2 % (value for the G10N6P12 formulation).

Thus, since the chosen cement pieces that were analysed were macroscopically representative of the total cement cylinder and that the deviation values between real and theoretical values of inorganic content are low, generically, the produced bone cements can be considered as homogeneous materials, and that the high difference on the density of the applied chemicals was not significant for the homogenization of the produced cements. This can also prove that the used mixture method of the chemicals to produce the bone cement formulations was successfully performed.

Table 6 - Obtained values from morphological characterization of the produced composite cements.

Cement Composites	CP wt.%	Nitrogen Adsorption			SEM	Helium Pycnometry	Indirect Calculation	
		BET Surface Area, $m^2.g^{-1}$	BET Average Pore Diameter, Å	BJH Pore Volume, $cm^3.g^{-1}$, $\times 10^4$	Average Pore Diameter, Mm	Real Density, $g.cm^{-3}$	Bulk Density, $g.cm^{-3}$	Porosity, %
G10N6P6	78	1.25±0.38	128.31±75.17	36.43±11.08	294.11±105.40	2.24±0.06	0.28±0.04	87.46±0.36
G10N6P12	72	1.19±0.23	152.33±12.59	46.51±7.21	308.82±143.51	2.26±0.04	0.39±0.04	82.71±0.27
G10N18P6	66	1.45±0.13	172.24±14.79	61.92±0.33	233.16±135.59	2.21±0.07	0.54±0.34	75.55±0.78
G10N18P12	60	1.36±0.16	143.39±98.17	50.57±38.99	188.24±150.67	2.13±0.02	0.33±0.02	84.47±0.15
G15N12P9	64	1.47±0.30	178.08±63.30	62.82±9.74	323.53±65.77	2.13±0.01	0.46±0.03	78.35±0.07
G20N6P6	68	1.09±0.06	148.33±0.84	40.30±2.61	189.54±99.12	2.03±0.16	0.38±0.07	81.17±1.51
G20N6P12	62	1.04±0.42	179.48±35.52	44.51±9.58	267.65±120.87	1.68±0.37	0.34±0.04	79.18±4.66
G20N18P6	56	2.16±0.70	171.43±29.55	94.95±46.18	284.92±154.13	1.67±0.60	0.44±0.13	71.73±10.20
G20N18P12	50	1.67±0.37	156.87±5.63	65.17±11.96	104.28±49.16	1.98±0.02	0.40±0.10	79.75±0.21

CP: Calcium phosphate; G: Gelatine; N: Na_2HPO_4 (accelerator); P: SFM processed pieces

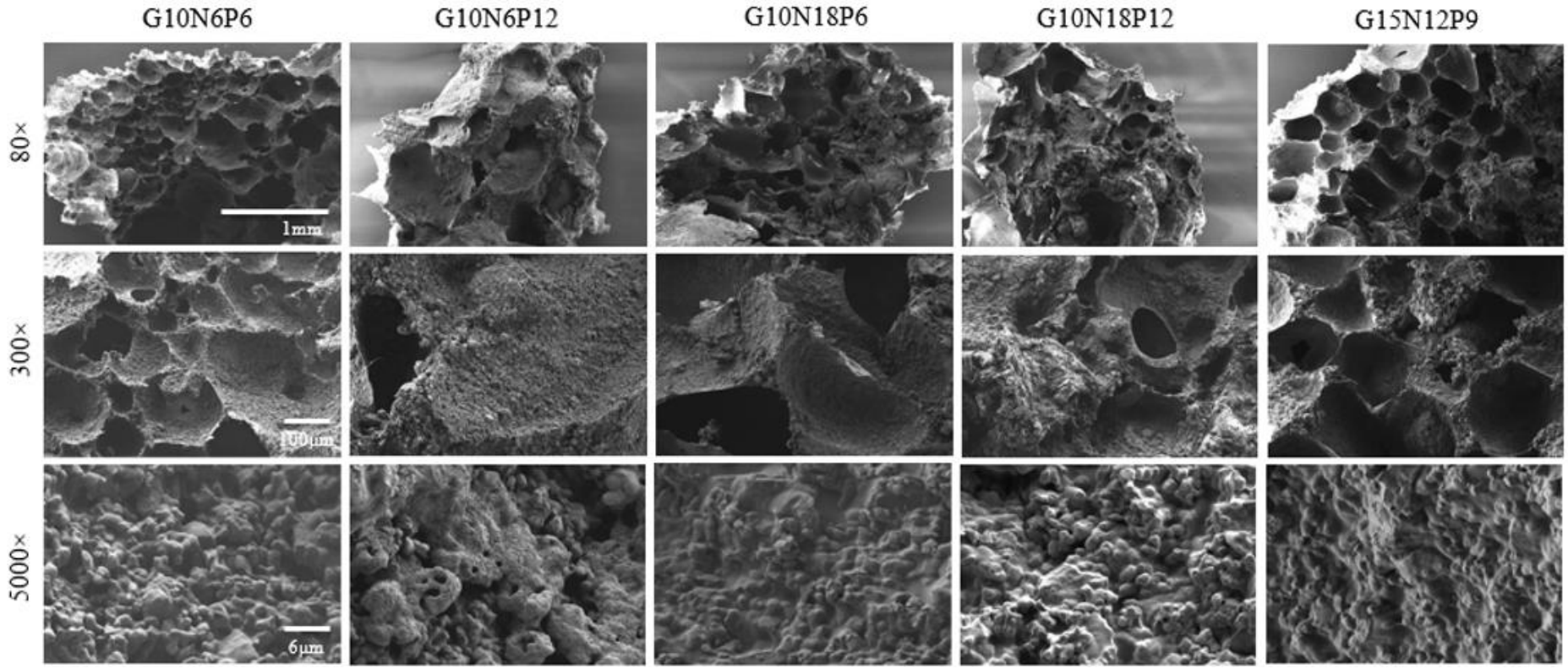

Figure 11 - SEM photographs of representative parts of the produced cements with 10 and 15 wt. % of gelatine. The presented magnifications from top to down lines are 80×, 300× and 5000×, respectively. Scale bar from top to down: 1mm, 100μm and 6μm, respectively.

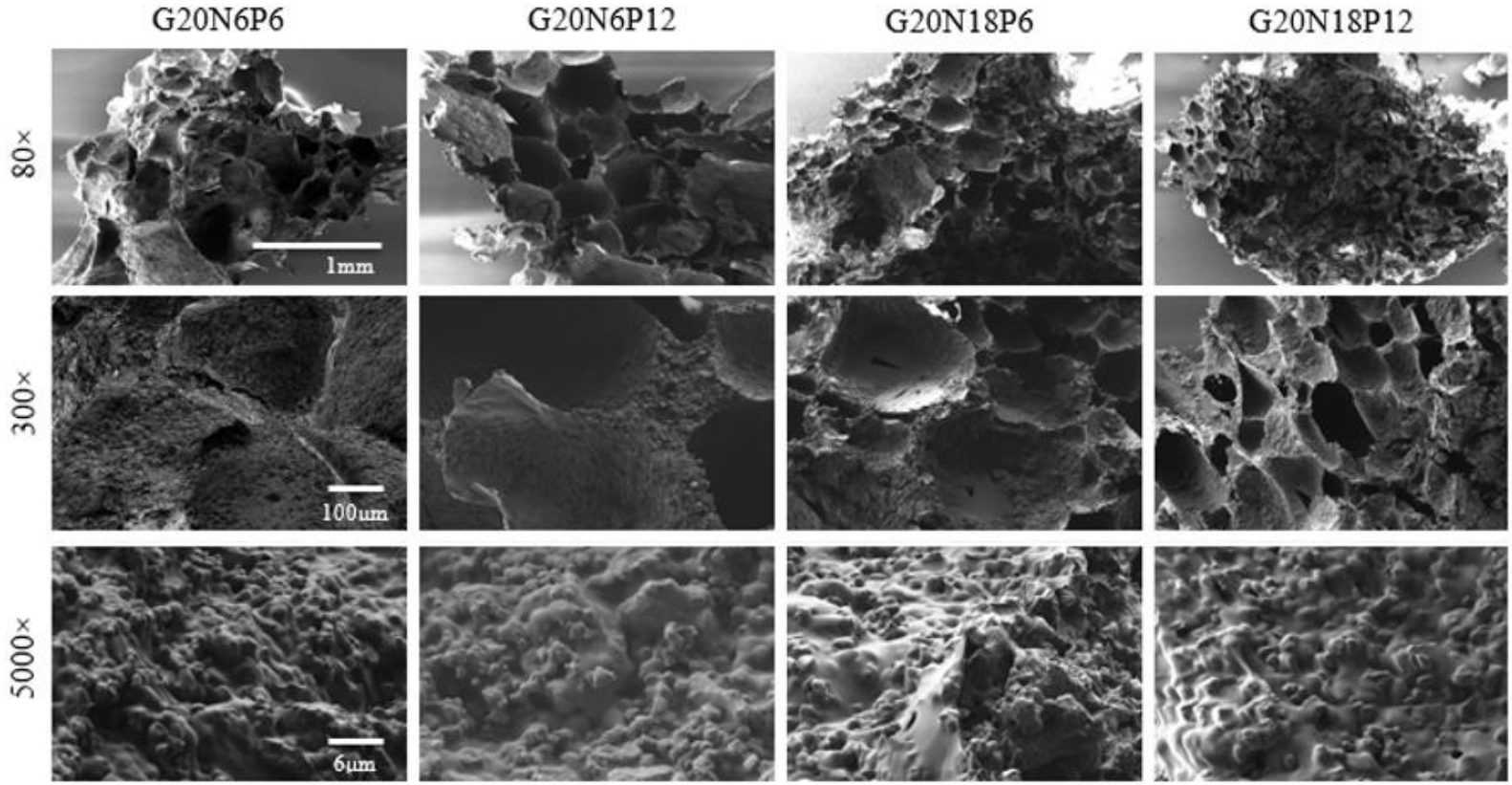

Figure 12 - SEM photographs of representative parts of the produced cements with 20 wt. % of gelatine. The presented magnifications from top to down lines are 80×, 300× and 5000×, respectively. Scale bar from top to down: 1mm, 100μm and 6μm, respectively.

3.3.3. Mechanical analysis

Compressive strength and Young's modulus of the produced cements were evaluated, using an oedometer, applying increasing loads into the cement samples. In Figure 13, it is shown the calculated values for Young's modulus at 2% strain and compressive strength at ultimate stress, respectively, for all produced cements. On Appendix G, it is shown an example of a curve of stress (MPa) *vs* strain (mm/mm) of the composite G20N6P6.

The previous graphics are organized by gelatine content to an easier visual analyse. The four formulations presented at blank were produced with 10 wt. % of gelatine, and the four formulations presented at dark grey were produced with 20 wt.%. In the middle (light grey) is the formulation with 15 wt.%. The cement G20N6P6 revealed the highest Young's modulus (45.25±22.33MPa), however, it also revealed the highest deviation value. The cement with lower Young's modulus was G10N6P6 (1.56MPa). It was not physically possible to perform the mechanical assay for its duplicate, since the material was completely brittle when in contact with the first load on the oedometer test.

The samples G10NIP12 and G10N18P12 had values near zero. It is generically visible that materials produced with higher content of gelatine revealed a higher Young's modulus, which was expected, since gelatine enhances material elasticity, improving its fracture toughness. Gelatine was also used in previous studies mixed with CPCs in order to enhance mechanical properties (Montufar *et al.*, 2010; Bankoff, 2012). It is, still, possible to state that materials with lower content of gelatine are more homogeneous, considering mechanical analyse.

The content of processed pieces or accelerator did not have any influence on the Young's modulus of the bone cements.

The material that revealed the highest compressive strength was the G15N12P9 (2.03±0.07 MPa), and the material with lowest value was, once again, the G10N6P6 (0.27MPa). In this graphic, it is also possible to see, generically, that materials with higher content of gelatine have higher compressive strength, which also agrees with literature (Montufar *et al.*, 2010; Bankoff, 2012). One interesting feature of the produced composite cements is that they revealed Young's modulus and compressive strengths similar or higher to the values of some commercially available CPCs, namely ChronOS®Inject (54 MPa and 0.81 MPa, respectively) and Ostim® (6MPa and 0.24MPa, respectively) (Van Lieshout *et al.*, 2011).

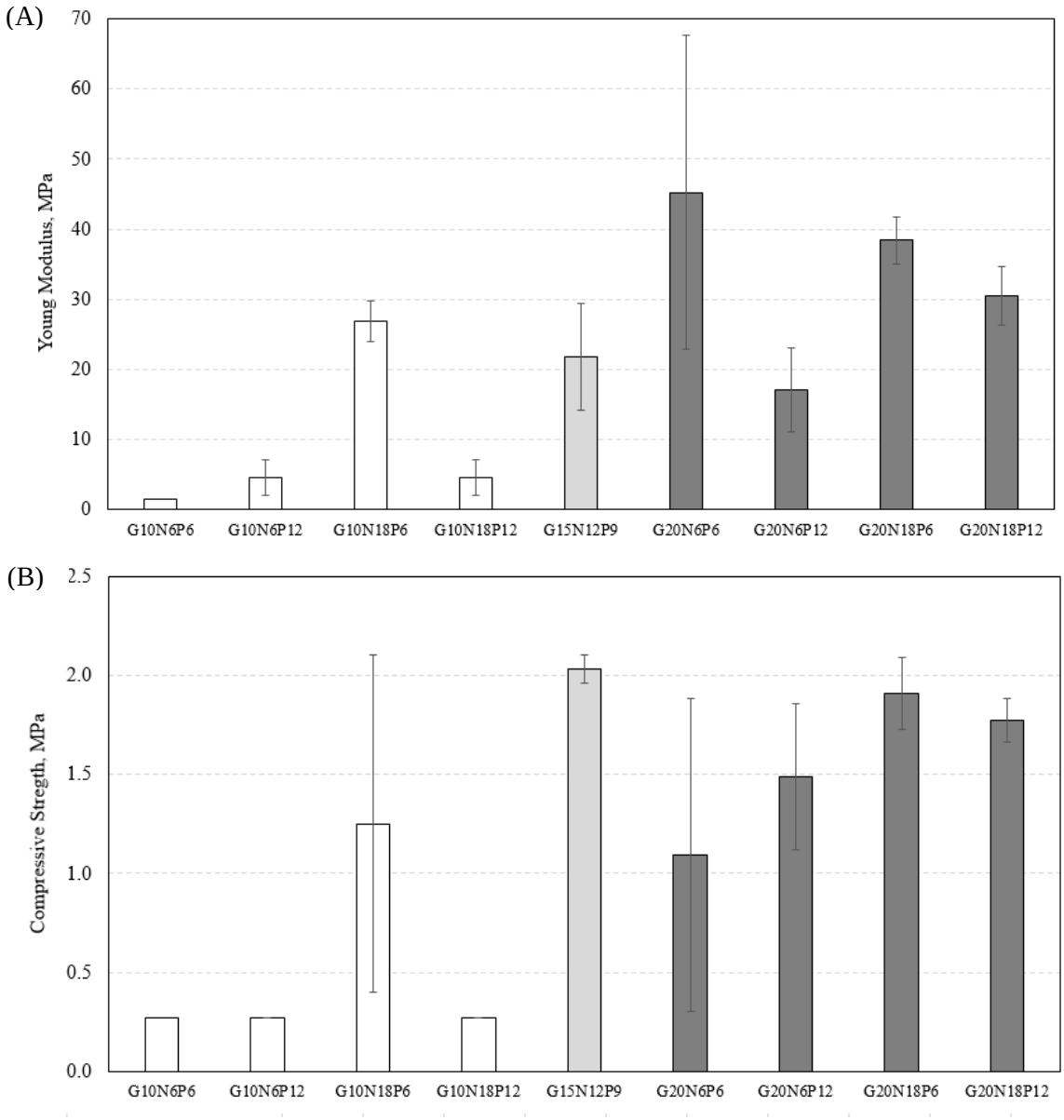

Figure 14 – Mechanical performance of the composite cements: Young's Modulus, MPa, (A) and compressive strength, MPa (B)

3.3.4. Dexamethasone release profile

In order to study the drug delivery of some of the produced cements were selected the two formulations that revealed the best mechanical performance, considering the highest values of Young's modulus and compressive strength: G20N18P6 and G15N12P9, respectively. These formulations were produced as previously explained, mixing the pre-setting cement with dexamethasone (DXMT) powder (0.5 wt.%). In Figure 14, it is possible to observe the releasing behaviour of these two cements along the first eight days of assay. In Figure 14A, it is shown the release of mg of dexamethasone per each g of composite cement. Generically, it is clear that the two

release profiles are very similar, with exception to the last hour, where the composite G20N18P6 reveals a higher releasing rate (also visible in Figure 14B). Basically, on the first eight days of contact, it was released 2 mg of DXMT for 1 g of composite cements. The total of DXMT released in this time interval was 0.59±0.05 g and 0.51±0.07 g, which was approximately 40% of the total initial mass (Figure 14B).

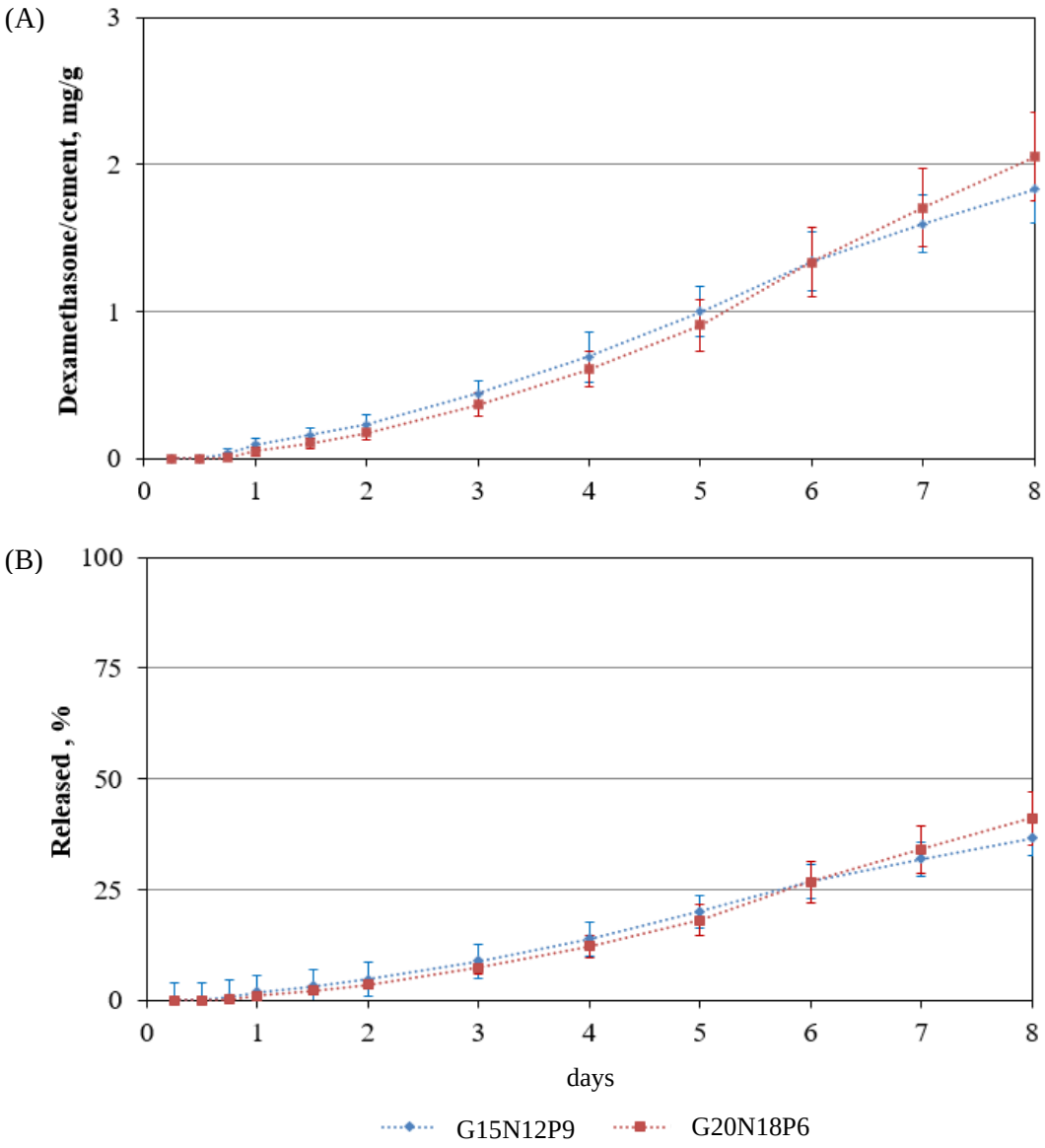

Figure 15 – DXMT release profile with the cements that revealed the better mechanical performance along the first eight days of assay: DXMT/cement, mg/g, released (A) and total Released DXMT, % (B)

It was stated that CPCs are promising matrices for osteogenic drug loading, since it can be delivered for a long time, being biologically active and promoting differentiation of mesenchymal stem cells into osteoblasts and being compatible, for instance, with the bone regeneration (period of time) towards a fracture (Forouzandeh *et al.*, 2013).

Based on these values, it is predictable that the DXMT would be completed released in approximately 20 - 22 days later, assuming a proportional releasing rate over time. However, this conclusion must be taken without absolutely certainly, since the release behaviour may not be proportional over time. It was seen in the literature that with other similar DXMT-loaded CPCs, the total release occurred along approximately a month, a relatively long period of time which is an important advantage for hard tissue engineering applications (Forouzandeh *et al.*, 2013).

3.3.5. Hemocompatibility assays

Hemocompatibility assays were performed to all cement formulations with three different methods: i) direct contact without SBF treatment, ii) indirect contact without SBF treatment and iii) indirect contact with SBF treatment, as can be seen on the next table that shows the haemolytic index, %, per cement formulation and per method (Kokubo *et al.*, 2006; Jones *et al.*, 2001; Sepulveda *et al.*, 2002). The difference among the applied methods was already explained on the methods section of this thesis.

Table 7 – Hemolytic index, %, per cement formulation and per method.

Cements formulations	**Hemolytic index, %**		
	Without treatment	**With SBF treatment**	
	Direct contact		**Indirect contact**
G10N6P6	11.30±4.78	3.84±0.14	-0.18±0.03
G10N6P12	7.43±1.43	4.52±0.03	0.07±0.67
G10N18P6	27.51±0.04	4.28±0.29	-0.38±0.00
G10N18P12	29.69±2.86	4.79±0.29	-0.33±0.04
G15N12P9	-1.63±0.02	4.49±0.43	-0.32±0.04
G20N6P6	14.44±11.83	3.77±0.09	-0.24±0.16
G20N6P12	-	4.61±0.03	-0.18±0.12
G20N18P6	-	3.75±0.29	0.03±0.18
G20N18P12	-	4.10±0.04	0.27±0.11
Hemolytic Behaviour (ASTM F756-00, 2008)	>5% Hemolytic	2% - 5% Slightly Hemolytic	< 2% Not-Hemolytic

The direct contact without SBF treatment method was based on previous works, since it was reported that calcium phosphate cements that were not α-TCP, do not have apatite formation on their surfaces when immersed into SBF, or even *in vivo* assays. It was explained that non α-TCP cements present high resorbability which could be the reason for the non-formation of apatite layers. It is also known that a material able to form

apatite layers on its surface can bond to living bone easily (Kokubo *et al.*, 2006). About the last three presented cement formulations it was not possible to assess their haemolytic index since they revealed a too much gelatinous appearance and they presented a too small liquid phase that did not enable the assay. This can be due to the high content on gelatine (20 wt.%). All hemolytic index assessed by this method are higher than 5% (hemolytic, according to ASTM F756-00 (2008)) (with exception of the cement G15N12P9 that revealed a negative value, no reason was found for this), which means that, according to this method, any of the produced cements are compatible with blood, despite the content of gelatine, which is a biocompatible polymer.

Since the examination of apatite formation on the surface of a material in SBF is useful for predicting the *in vivo* bone bioactivity qualitatively and quantitatively (Kokubo *et al.*, 2006), it was also performed an indirect contact assay with SBF immersion (Jones *et al.*, 2001; Sepulveda *et al.*, 2002). Here, it was possible to see that all obtained values are lower than 2% (particularly closer to 0%) meaning that all the cements, according to this method, are not hemolytic (ASTM F756-00 (2008)), being theoretically compatible with human blood. There are, actually, negative values, which means that these formulations should be the most biocompatible with the blood. It was noted that when the samples were immersed into SBF, there was a dissolution of the cements and possibly some solubilized gelatine loss. However, analysing the direct method also with SBF, it is possible to observe that all the hemolytic index values, are between 2% and 5%, meaning that all the cements are slightly hemolytic (ASTM F756-00 (2008)), despite there is no relation between cement composition and obtained index value. It is possible to conclude that with the different employed methods it was obtained different results to analyse the hemocompatibility behaviour of the cements: when using the direct contact method without SBF treatment, all the cements were classified as hemolytic (with exception to the intermediate formulation that revealed a negative value); when using the indirect contact method also without SBF treatment, all the cements were classified as slightly hemolytic; and finally when using the SBF treatment, all the cements behaved as not-hemolytic. Hemocompatibility assays were not conclusive. However, should be performed additional assays to these cement formulations to conclude about their cytotoxicity and to access if they induce any inflammatory response (some of this assays could eventually be performed to the formulations produced with DXMT).

4. Conclusion

The main objective of this work was to develop calcium-phosphate/gelatine-based bone cement composites with the incorporation of grinded SFM pieces, in order to fill a bone defect. This incorporation was performed in order to enhance final cement properties, such as morphological (surface area, pore diameter, macroporosity and bulk and real densities), mechanical (Young's modulus and compressive strength), hemocompatibility and to enable controlled drug release. Monoliths, pieces and final composite cements were analyzed.

SFM-processed pieces of PCL/SBA-15 silica nanoparticles (92:8 + 98 molar % of GF) were effectively incorporated into cement formulations after a selection process of PCL particle size, SBA-15 silica nanoparticles weight percent composition and GF molar concentration. It was proved that these pieces are highly porous (73.28±0.07) biomaterials. It was possible to conclude about SFM pieces homogeneity, high surface area (1.93±0.96 $m^2.g^{-1}$) and to calculate the average pore diameter of the pieces as 196.17±75.42 μm which is in the range of values found in the literature for commercially available calcium phosphate cements.

The general mixing time of the chemicals for the cement formulations was about 7.5±0.5 minutes. Setting time is not independent of mixing time since it was visible that on the final seconds of the mixing step granules of gelatine started setting. It is possible to conclude that all produced cement formulations behaved as fast-setting. The main limitation is the mixing time close value to the setting time, which can compromise surgeon manipulation when filling a bone defect, since he may not be quick enough to mould the pre-setting cement to the defect (particularly for complicate shapes). Another problem concerning the setting time of the produced cements is that gelatine granules may start setting during mixing time, which totally compromises cement application. Cements general water evaporation time was about 12 days at 37ºC. The water evaporation time will, certainly, be different if applied on human/animal body since the physiologic conditions are different to those of the *in vitro* assay. *In vivo* assays should also be performed in future studies, for example, using the produced calcium phosphate/gelatine-based bone cements as an osteoconductive filler of bone defects of a sheep leg (Appendix B illustrates an example for this application).

It was expected that, based on other studies, SFM pieces would enhance surface area of the produced cements. However, it was seen that BET surface area was lower for

formulations with higher content of SFM pieces (12 wt.%) and higher for formulations with lower content (6 wt.%). One possible cause for this might be the reduction of surface area of the SFM pieces when grinded. Surface area was synergistically improved in formulations with higher content in gelatine and accelerant (Na_2HPO_4).

It was proved that cements with higher content on calcium phosphate (78 wt. % and 72 wt. %) are highly porous biomaterials, revealing values of porosity higher than 82%. They also revealed higher values of real density when compared to other formulations. On the other hand, gelatine and SFM pieces did not reveal a direct impact on the values of density or porosity. Generically, the values of porosity of the produced cements are higher when compared to some commercially available calcium phosphate cements. Through SEM, it was visible that produced cements presented highly porous coral-type structures. All the produced cements revealed to be suitable candidates for hard tissue engineering applications from the morphological point of view, namely for bone defect fill, since they are in the suitable range for these type of application with macropores proper for new bone tissue ingrowth and mesopores, which induce biodegradation (namely bulk degradation), good blood diffusion and an effective loading/release of bioactive compounds. The roughness of the surface is probably caused by the fast-setting of gelatine granules. SDT was useful, above all, to prove that cement formulations were homogeneously mixed and that the used mixing process for producing the bone cements was successful.

Cements produced with higher content of gelatine revealed, generically, higher mechanical properties. Once again, SFM pieces content did not present any significant impact on these features. Young's modulus and compressive strength of some of the cements were higher than some commercial calcium phosphate cements.

Regarding osteogenic drug delivery profile of the two cements with the highest mechanical performance, it was possible to see that 40% of the total initial DXMT mass was delivered along the first eight days of assay, which means that it could be completed delivered along ~21 days, estimation based on the release profile, which also agrees with literature values for similar cases. This time interval is considered a relatively long period of time compatible with bone regeneration.

Hemolytic index of cement formulations revealed different results depending on the employed method. It was admitted that this analyse was not conclusive and that further research should be performed, such as perform hemocompatibility assays to cement formulations with DXMT (since this one is an anti-inflammatory osteogenic drug).

For future works, could be interesting to increase the SFM pieces content (up to 20 or 25 wt.%) and to load SFM pieces with DXMT trough supercritical CO_2 solvent impregnation/deposition (SSID) method instead of the employed method of drug mixing with the pre-setting cement, and to compare the release profiles. Finally, perform injection assays with the cement formulations immediately after mixing process, in order to reproduce a surgery. Assays of rheology could also be a viable alternative. In last instance, it would be great to test the cement formulation *in vivo*, for example, performing a surgery similar to the one that was performed with Bonelike that can be consulted on APPENDIX A and B.

5. References

1. ASTM C 1341-00 – Flexural Testing of Fiber-Reinforced Ceramics (2002)
2. ASTM C 226-12 – Standard Specification for Air-Entraining Additions for Use in the Manufacture of Air-Entraining Hydraulic Cement PA (2012)
3. ASTM D790 – Standard Test Methods for Flexural Properties of Unreinforced and Reinforced Plastics and Electrical Insulating Materials (1990)
4. ASTM E399 – Standard Test Method for Linear-Elastic Plane-Strain Fracture Toughness Kic of Metallic Materials (1997)
5. ASTM F451 – Standard Specification for Acrylic Bone Cement, ASTM International, West Conshohocken, PA (2008)
6. ASTM F756-00 – Standard Practice for Assessment of Haemolytic Properties of Materials (2008)
7. Atayde L., Substitutos Ósseos Para Regeneração do Tecido Ósseo: Estudos In Vivo e Futuras Aplicações Clínicas Em Medicina Veterinária, MSc Thesis, ICBAS (2013)
8. Balmayor E., Griensven M., Drug Delivery to Bony Tissue, Advanced Drug Delivery Reviews, 2015
9. Bankoff D.P.A., Biomechanical Characteristics of the Bone, Human Musculoskeletal Biomechanics, InTech, 2012
10. Bhamidipati M., Scurto A.M., Detamore M.S., The future of carbon dioxide for polymer processing in tissue engineering, Tissue Engineering: Part B, 19 (2013) 221-232
11. Blom E.J., Klein-Nulend J., Wolke J.G.C., van Waas M.A.J., Driessens F.C.M., Burger E.H., Transforming growth factor-β 1 incorporation in a calcium phosphate bone cement: material properties and release characteristics, Journal Biomedical Material Research, 59 (2002) 265–272
12. Boanini E., Panzavolta S., Rubini K., Gandolifi M., Bigi A., Effect of Strontium and Gelatin on the Reactivity of α-Tricalcium Phosphate, Acta Biomaterialia, 6 (2010) 936-942
13. Bohner M., Baroud G., Injectability of calcium phosphate pastes, Biomaterials, 26 (2005) 1553–1563
14. Bohner M. Calcium orthophosphates in medicine: From ceramics to calcium phosphate cements, Injury, 31 (2000) 37-47
15. Bohner M., Design of ceramic-based cements and putties for bone graft substitution, European Cell and Materials, (2010) 1–12
16. Bohner M., Baroud G., Injectability of calcium phosphate pastes. Biomaterials, 26 (2005) 1553–1563

17. Bohner M., Physical and chemical aspects of calcium phosphates used in spinal surgery, European Spine Journal, 10 (2001) 114–121
18. Bohner M., Reactivity of calcium phosphate cements, Journal of Materials Chemistry, 17 (2007) 3980–3986
19. Boland E.D., Coleman B.D., Barnes C.P., Simpson D.G., Wnek G.E., Bowlin G.L., Electrospinning polydioxanone for biomedical applications, Acta Biomaterialia, 1 (2005) 115-123
20. Bonnila C.E.P., Trujillo S., Demirdogen B., Perilla J.E., Elcin Y.M., Ribelles J.L.G., New porous polycaprolactone-silica composites for bone regeneration, Materials and Engineering C, 40 (2014) 418 – 426
21. Bose S, Saha S.K., Synthesis and characterization of hydroxyapatite nanopowders by emulsion technique, Chemistry of Materials., 15 (2003) 4464–4469
22. Bose S., Tarafder S., Edgington J., Bandyopadhyay A., Calcium phosphate ceramics in drug delivery, Journal of the Minerals, metals and Materials Society, 63 (2011) 93–98
23. Bose S., Tarafder S., Calcium phosphate ceramic systems in growth factor and drug delivery for bone tissue engineering: A review, Acta Biomaterialia, 8 (2012) 1401-1421
24. Braga, M.E.M., Costa,V.P., Pereira, M.J.T., Fiadeiro, P.T., Gomes, A.P.A.R., Duarte, C.M.M., de Sousa, H.C., Effects of operational conditions on the supercritical solvent impregnation of acetazolamide in Balafilcon, A commercial contact lenses, International Journal of Pharmaceutics 2 (2011) 231–243
25. Bucholz R.W., Nonallograft osteoconductive bone graft substitutes, Clinic Orthopaedics and Related Research 2002:44–52
26. Bose S., Tarafder S., Calcium phosphate ceramic systems in growth factor and drug delivery for bone tissue engineering: A review, Acta Biomaterialia, 8 (2012) 1401-1421
27. Bueno C. Z., Moraes A. M., de Sousa H.C., Braga M. E. M., Effects of supercritical carbon dioxede processing on the properties of chitosan-alginate membranes, Journal of Supercritical Fluids, 112 (2016) 128-135
28. Burg K.J., Porter S., Kellam J.F., Biomaterial developments for bone tissue engineering, Biomaterials, 21 (2000) 2347-2359
29. Carrodeguas R.G., De Aza S., α-Tricalcium phosphate: Synthesis, properties and biomedical applications, Acta Biomaterialia, 7 (2011) 3536-3546
30. Champeau M., Thomassin J.-M., Tassaing T., Jérôme C., Drug loading of polymer implants, Journal of Controlled Release, 209 (2015) 248-259
31. Chen B-K., Shih C-C., Chen A.F., Ductile PLA nanocomposites with improved thermal stability, Composites: Part A, 43 (2012) 2289-2295
32. Cheung H., Lau K., Lu T., Hui D., A critical review on polymer-based bio-engineered materials for scaffold development, Composites Part B: Engineering, 38 (2007) 291–300

33. Chin C.S., Litle V., Yun J., Weiser T., Swanson S.J., Airway stents, The Annals of Thoracic Surgery, 6 (2008) 785 - 792
34. Chow L.C., Takagi S., A natural bone cement - A laboratory novelty led to the development of revolutionary new biomaterials, Journal of Research of the National Institute of Standards and Technology, 106 (2001) 1029 –1033
35. Chow L.C., Next generation calcium phosphate-based biomaterials, Dental Mater Journal., 28 (2009) 1-10
36. Churro R., Supercritical foaming/mixing on the preparation of PCL/mesoporous silica based composites for hard tissue engineering applications, MSc Thesis, Universidade de Coimbra, Portugal (2015)
37. Churro R.M., Rosa A.S., Correia A. A., Braga E.M., de Sousa H.C., Supercritical CO_2 foamong/mixing for the preparation of plasticized porous PLC/SBA-15 composite biomaterials. II. Effects of operational conditions and relative compositions of additives, Journal of Supercritical Fluids (2016)
38. Costa-Pinto A.R., Reis R.L., Neves N.M., Scaffolds based bone tissue engineering: The role of chitosan, Tissue Engineering: Part B, 17 (2011) 1-17
39. Cui X., Zhang Y., Wang H., Gu Y., Li L., Zhou J., Zhao S., Huang W., Zhou N., Wang D., Pan H., Rahaman M.N., An injectable borate bioactive glass cement for bone repair: Preparation, bioactivity and setting mechanism, Journal of Non-Crystallize Solids, 432 (2015) 150-157
40. De Matos M.B.C., Puga A.M., Alvarez-Lorenzo C., Concheiro A., Braga M.E.M., de Sousa H.C., Osteogenic poly(ε-caprolactone)/poloxamine homogeneous blends prepared by supercritical foaming, International Journal of Pharmaceutics, 479 (2014) 11-22
41. De Matos M.B.C., Piedade A.P., Alvarez-Lorenzo C., Concheiro A., Braga M.E.M., de Sousa H.C., Dexamethasone-loaded poly(ε-caprolactone)/silica nanoparticles composites prepared by supercritical CO2 foaming/mixing and deposition, International Journal of Pharmaceutics, 456 (2013) 269-281
42. Denaro L., Longo U. G., Denaro V., Vertebroplasty and kyphoplasty: Reasons for concern?, Orthopedic Clinics North America, 40 (2009) 465-471
43. Dickman C.A., Fessler R.G., MacMillan M., Transpedicular screw-rod fixation of the lumbar spine: operative technique and outcome in 104 cases, Journal of Neurosurgery, 77 (1992) 860–870
44. Dorozhkin S.V., Calcium orthophosphate cements for biomedical application, Journal of Materials Science, 43 (2008) 3028–3057
45. dos Santos L. A., de Oliveira L. C., Rigo E. C. S., Carrodeguas R. G., Boschi A. O., de Arruda A. C. F, Influence of Polymeric Additives on the Mechanical Properties of α-Tricalcium Phosphate Cement, Materials Science Forum, 25 (1999) 99-102

46. Duarte F., Santos J. D., Afonso A., Medical applications of Bonelike® in Maxillofacial Surgery, Materials Science Forum, 37 (2004) 455-456
47. Dubruel P., Vlierberghe S. V., Biomaterials for Bone Regeneration – Novel Techniques and Applications, Woodhead Publishing, 36 (2014) 25 - 26
48. Eckert C., Knutson B., Debenedetti P., Supercritical fluids as solvents for chemical and materials processing. Nature, 383 (1996) 313–383
49. Espanol M., Perez R.A., Montufar E.B., Marichal C., Sacco A., Ginebra M.P., Intrinsic porosity of calcium phosphate cements and its significance for drug delivery and tissue engineering applications, Acta Biomaterial, 5 (2009) 2752-2762
50. Forouzandeh A., Hesaraki S., Zamanian A., The Releasing Behavior and In Vitro Osteoinductive Evaluations of Dexamethasone-Loaded Porous Calcium Phosphate Cements, Ceramics International, 40 (2014) 1081-1091
51. Gautam S., Dinda A., Mishra N., Fabrication and Characterization of PCL/Gelatin Composite Nanofibrous Scaffold for Tissue Engineering Applications by Electrospinning Method, Materials Science and Engineering C., 33 (2013) 1228-1235
52. Groot K.D., Bioceramics of calcium phosphate, Journal of Clinical Engineering 9 (1984) 52
53. Habraken W.J., Zhang Z., Wolke J.G., Grijpma D.W., Mikos A.G., Feijen J., Introduction of enzymatically degradable poly(trimethylene carbonate) microspheres into an injectable calcium phosphate cement, Biomaterials, 29 (2008) 2464–2476
54. Harrison, K., Introduction to polymeric scaffolds for tissue engineering, Biomedical Polymers, 1 (2007) 1–32
55. Huang T.H., Shie M.Y., Kao C.T., Ding S.J., The effect of setting accelerator on properties of mineral trioxide aggregate, Journal of Endodontics, 34 (2008) 590-593
56. Ikawa N., Kimura T., Oumi Y., Sano T., Amino acid containing amorphous calcium phosphates and the rapid transformation into apatite, Journal of Materials Chemistry, 19 (2009) 4906–4913
57. Jain K.K., Drug delivery systems - an overview, Methods in Molecular Biology, 437 (2008) 1–50
58. Jain N.K, Rana A.C., Jain S.K., Brain drug delivery system bearing dopamine hydrochloride for effective management of parkinsonism, Drug Development Industrial Pharmacy, 24 (1998) 671-675
59. Kokubo T., Bioactive glass ceramics: properties and applications, Biomaterials, 12 (1991) 155-163
60. Kokubo T., Kim H.M., Kawashita M., Novel Bioactive Materials with Different Mechanical Properties, Biomaterials, 24 (2003) 2161-2175

61. Lai P.L., Chen L.H., Chen W.J., Chu I.M., Chemical and Physical Properties of Bone Cement for Vertebroplasty, Biomedical Journal, 36 (2013) 162 -167,
62. Lewis G., Injectable bone cements for use in vertebroplasty and kyphoplasty: State of-the-art review, Journal of Biomedical Materials Research Part B: Applied Biomaterials, 76 (2006) 456-468,
63. Lee J.H, Kim J.H., Oh S.H., Kim S.J., Hah Y.S., Park B.W., Kim D.R., Rho G.J., Maeng G.H., Jeon R.H., Lee H.C., Kim J.R., Kim G.C., Kim U.K., Byun J.H., Tissue-engineered bone formation using periosteal-derived cells and polydioxanone/pluronic F127 scaffold with pre-seeded adipose tissue-derived CD146 positive endothelial-like cells, Biomaterials, 32 (2011) 5033-5045
64. Lee L.J., Zeng C., Cao X., Han X., Shen J., Xu G., Polymer nanocomposite foams, Composites Science and Technology, 65 (2005) 2344-2363
65. LeGeros RZ., Calcium phosphate-based osteoinductive materials, Chemical Reviews, 108 (2008) 4742–4753
66. Lidgren L., Bodelind B., Moller J., Bone Cement Improved by Vacuum Mixing and Chilling, Acta Orthopaedica Scandinavica, 58 (1987) 27-32
67. Lieberman I.H., Togawa D., Kayanja M.M., Vertebroplasty and kyphoplasty: Filler materials. Spine Journal, 5 (2005) 305-316
68. Liu C., Xia Z.,Czernuszk J.T., Design and development of three-dimensional scaffolds for tissue engineering, Chemical Engineering Research Design, 85 (2008) 1051-1064
69. Liu K., Kiran E., High-pressure solution blending of poly(ε-caprolactone) with poly(methyl methacrylate) in acetone + carbon dioxide, Polymer, 49 (2008) 1555-1561
70. Liu Y., de Groot K, Hunziker E. BMP-2 liberated from biomimetic implant coatings induces and sustains direct ossification in an ectopic rat model, Bone, 36 (2005) 745–757
71. Loeffel M., Ferguson S.J., Nolte L.P., Kowal J.H., Vertebroplasty: Experimental characterization of polymethylmethacrylate bone cement spreading as a function of viscosity, bone porosity, and flow rate, Spine, 33 (2008) 1352-1359
72. Maitra A. Calcium phosphate nanoparticles: second-generation nonviral vectors in gene therapy, Expert Review of Molecular Diagnostic, 5 (2005) 893–905
73. Manuel C., Foster M., Monteiro F, Ferraz M., Doremus R.H, Bizios R., Preparation and characterization of calcium phosphate nanoparticles, Key Engineering Materials, (2004) 254–256
74. Mathis M.M., Petri M., Naff N., Percutaneous Vertebroplasty Treatment of Steroid-Induced Osteoporotic Compression Fractures, Arthritis and Rheumatism, (1998) 171-175
75. Middleton J.C, Tipton A.J., Synthetic biodegradable polymers as orthopedic devices, Biomaterials, 23 (2000) 2335-2346

76. Montufar E. B., Traykova T., Schacht E., Ambrosio L., Santin M., Planell J. A., Ginebra M.P., Self-hardening calcium deficient hydroxyapatite/gelatine foams for bone regeneration, Journal of Mater Science, 21 (2010) 863-869
77. Nalawade S.P., Picchioni F., Janssen L.P.B.M, Supercritical carbon dioxide as a green solvent for processing polymer melts: Processing aspects and applications, Progress in Polymer Science 31 (2006) 19-43
78. Novotny L., Ctha M., Rauser P., Hep A., Misik Jan., Necas A., Vondrys D., Novel biodegradable polydioxanone stents in a rabbit airway model, The Journal of Thoracic and Cardiovascular Surgery, 2 (2012) 437-444
79. Palmer L.C., Newcomb C.J., Kaltz S.R., Spoerke E.D., Stupp S.I., Biomimetic systems for hydroxyapatite mineralization inspired by bone and enamel, Chemical Reviews, 108 (2008) 4754–4783
80. Ray J.A., Doddi N., Regula D., Williams J.A., Melveger A., Polydioxanone (PDS), a novel monofilament synthetic absorbable suture, Surgery Gynecol Obstet, 153 (1981) 497–507
81. Renders G.A.P., Mulder L., van Ruijven L.J., van Eijden T.M.G.J, Porosity of human mandibular condylar bone, J. Anat., 210 (2007) 239-248
82. Rey C., Calcium phosphate biomaterials and bone mineral: Differences in composition, structures and properties, Biomaterials 11 (1990) 13–15
83. Rosa A.B.S., Poly (ε-caprolactone)/SBA-15 composite biomaterials plasticized with greener additives, MSc Thesis, Universidade de Coimbra, Portugal (2013)
84. Salgado A.J., Coutinho O.P., Reis R.L., Bone tissue engineering: state of the art and future trends, Macromolecular Bioskin, 4 (2004) 743 - 765
85. Sauceau M., Fages J., Common A., Nikitine C., Rodier E., New challenges in polymer foaming: A review of extrusion processes assisted by supercritical carbon dioxide, Progress in Polymer Science, 36 (2011) 749-766
86. Shi Q.H, Wang J.F., Zhang J.P., Fan J., Stucky G. D., Rapid-Setting, Mesoporous, Bioactive Glass Cements that Induce Accelerated In Vitro Apatite Formation, Advanced Materials, 10 (2005) 1038-1042
87. Shieh Y-T, Lai J-G, Tang W-L, Yang C-H, Wang T-L, Supercritical CO_2 intercalation of polyecaprolactone in layered silicates, Journal of Superctical Fluids 49 (2009) 385-393
88. Shum HC, Bandyopadhyay A, Bose S, Weitz D.A., Double emulsion droplets as microreactors for synthesis of mesoporous hydroxyapatite, Chemistry of Materials, 21 (2009) 5548–5555
89. Simões S. M. N., Veiga F., Ribeiro A. C. F., Figueiras A. R., Taboada P., Concheiro A., Lorenzo C. A., Supramolecular gels of poly-a-cyclodextrin and PEO-based copolymers for controlled drug release, European Journal of Pharmaceutics and Biopharmaceutics, 87 (2014) 579-588

90. Sun L., Chow L.C., Frukhtbeyn S.A., Bonevich J.E., Preparation and properties of nanoparticles of calcium phosphates with various Ca/P ratios, Journal of Research of the National Institute of Standard Technology 115 (2010) 243–255
91. Takahashi T., Tominaga T., Watabe N., Yokobori A.T., Sasada H., Yoshimoto T., Use of porous hydroxyapatite graft containing recombinant human bone morphogenetic protein-2 for cervical fusion in a caprine model, Journal of Neurosurgery, 90 (1999) 224–230
92. Tiwari G., Tiwari R., Sriwastawa B., Bhati L., Pandey S., Pandey P., Bannerjee S.K., Drug delivery systems: An updated review, International Journal Pharmaceutical Investigation, 2 (2012) 2-11
93. Unosson J.E., Persson C., Engqvist H., An evaluation of methods to determine the porosity of calcium phosphate cements, Journal of Biomedical Research Part B: Applied Biomaterials, 103 (2015) 62-71
94. Vaishya R., Chauhan M., Vaish A., Bone Cement, Journal of Clinical Orthopaedics and Trauma, 4 (2013) 157 163
95. Vallo C., Montemartini P., Fanovich M., López J., Cuadrado T., Polymethylmethacrylate-Base Bone Cement Modified with Hydroxyapatite, Journal of Biomedical Materials Research, 48 (1999) 150-158
96. Van Lieshout E.M.M, Van Kralinger G.H., El-Massoudi Y., Weinans H., Patka P., Microstructure and biomechanical characteristics of bone substitutes for trauma and orthopaedic surgery, BMC Musculosketal Disorders, (2011) 12-34
97. Verron E., Khaairoun I., Guicheux J., Bouler J.M., Calcium phosphate biomaterials as bone drug delivery systems: a review. Drug Discovery Today, 15 (2010) 547–552
98. Weir M.D., Xu H.H., High-strength, in situ-setting calcium phosphate composite with protein release, Journal of Biomed Materials Research, 85 (2008) 388–396
99. Yang S., Leong K-F., Du Z., Chua C-K., The design of scaffolds for use in tissue engineering Part 1. Traditional factors, Tissue Engineering, 7 (2001) 679-689
100. Zdravkov B.D., Cermák J. J., Sefara M., Janku J., Pore classification in the characterization of porous materials: A perspective, Central European Journal of Chemistry, 5(2) (2007) 385-395
101. Zhang J., Liu W., Gauthier O., Sourice S., Pilet P.,Rethore G., Khairoun K., Bouler J., Tancret F., Weiss P., A simple and effective approach to prepare injectable macroporous calcium phosphate cement for bone repair: Syringe-foaming using a viscous hydrophilic polymeric solution, Acta Biomaterial, 31 (2015) 326-338
102. Zhang J., Liu W., Schnitzler V., Tancret F., Bouler J. M., Calcium phosphate cements for bone substitution: Chemistry, handling and mechanical properties, Acta Biomaterialia, 10 (2014) 1035-1049

103. Zuo Y., Yang F., Wolke J., Li Y., Jansen J., Incorporation of biodegradable electrospun fibers into calcium phosphate cement for bone regeneration, Acta Biomaterialia, 6 (2010) 1238-1247

APPENDIX A – Information about Bonelike® Spherical Osteoconductive Granules

Bonelike is constituted by HA (67.7%), β-TCP (25,8%) and α-TCP(6.5%). One of the most used applications of Bonelike is when is necessary to perform a maxillofacial surgery. Duarte *et al.* reported that Bonelike is a synthetic bone graft designed to mimic the inorganic composition of the new bone. The process consists of liquid sintering hydroxyapatite in the presence of $CaO\text{-}P_2O_5$ (Calcium Oxide – Phosphorus Pentoxide) based glass. This cement can be used for a reconstruction of a bone defected after a cyst excision, once it was proved that the granules of Bonelike were almost completely surrounded by new bone after 6 months. Bonelike shows high biodegradability and was approved for clinical applications, such as implantology and maxillofacial surgery. In the clinical case of this study, after the cyst have been removed, Bonelike granules were carefully mixed with physiological solution, remixed with patients blood and placed in the bone defected area. A histological evaluation demonstrated continuous replacement by new bone, proving the osteoconductive capacity of this cement (extensive new bone formation around implanted granules), providing conditions for a healthy and fast rehabilitation. It was also observed resorption of these particles, which can be explained due to the presence of controlled contents of bioresorbable β and α Calcium Phosphate (Duarte *et al.*, 2004).

According to Atayde *et al.,* Bonelike was developed as a synthetic bone substitute and is composed of two different types of materials (HA and a glass base). After a thermic process, a modified HA with a secondary matrix of β-TCP and α-TCP is produced. Thus, it is classified as biphasic or triphasic calcium phosphate if β-TCP and α-TCP are considered separately. According to the Bonelike registered patent, β-TCP and α-TCP phases are dispersed homogenously on the HA matrix, which is responsible for an improvement on mechanical properties and bioactivity behaviour when compared to pure HA. Besides, HA/TCP proportions can be modified in order to control mechanical resistance and resorption rate. The inclusion of the glass base in the production process allows the incorporation of different ions, such as fluorine, magnesium or sodium, mimicking the natural inorganic composition of the human bone. In the same consulted study, it was referred that Bonelike was previously tested *in vitro* and *in vivo*, where was showed that osteoblasts have proliferate and produced an extracellular matrix, proving that Bonelike composition had a better performance when compared to isolated

HA. It was also possible for osteoblasts to adhere and to proliferate suggesting an enormous potential to be applied in hard tissue engineering. It was also referred *in vivo* tests in sheep, and a faster osteoformation with Bonelike than with pure HA. This kind of surgeries, also done in humans (typically in implantology in dental area), were performed by filling the bone defect with Bonelike granules. These spherical granules facilitate cement flow and are considered osteoconductive and osteointegrative (Atayde *et al.*, 2013).

Currently, Bonelike is commercially available in three different particle sizes: 250-500µm, 500-1000µm and 1000-4000 µm. Its application depends on the size of the bone defect and type of defect, concerning, for example, an oral cavity or a fracture in a long bone.

Bonelike osteoconductive granules were used to perform SFM preliminary assays, in order to have another suggestion of inorganic component besides SBA-15 silica nanoparticles. These results were not discussed in this thesis since the density of Bonelike (2.3 $g.cm^{-3}$) is much higher than the density of PCL (1.1 $g.cm^{-3}$), which did not allow a good physical mixture with the formation of heterogeneous SFM monoliths, where was perfectly visible two different phases with a Bonelike layer on the top of the cylinder sample. Since the main objective of producing these materials was to grind them and to incorporate into bone cements, it was obvious that the pieces would not become similar between them. According to Atayde *et al.* (2013), this type of Bonelike revealed a dimeter of particle between 250 - 500 µm, global pore area of 0.264 $m^2 g^{-1}$, global average pore diameter of 4.996 µm, global porosity of 48.93%, real density of 1.468 g cm^{-3} and an apparent density of 2.298 g cm^{-3}.

APPENDIX B – Bonelike® Spherical Osteoconductive Granules: Surgery to a Sheep

During the work developed in this thesis, it was possible to observe a surgery to two sheep using Bonelike.

It was performed two surgeries at the same time. Both of them consisted on the filling of a bone defect that was made by a Bosh drill. 1 – In one of the sheep it was performed two circular bone defects with a diameter of ~ 2 cm on the back of the animal – one hole was made in each iliac crest – load free critical defect. This defect was then filled by bulkier polygonal Bonelike granules (d ~ 1-4 mm). Since these one have bigger pores, they should be manipulated gently in order to not destroy the pores. This method was then compared to other auto-graft performed on the same animal. 2 – On the second sheep, it was performed 5 bone defects with ~ 0.5 cm each on the femur of the animal – load not-critical defect, as can be seen on the next figure. On the first nothing was put. On the second only thinner Bonelike (0.250-0.500mm). On the third, forth and fifth it was put thinner Bonelike mixed with staminal cells of human dental pulp.

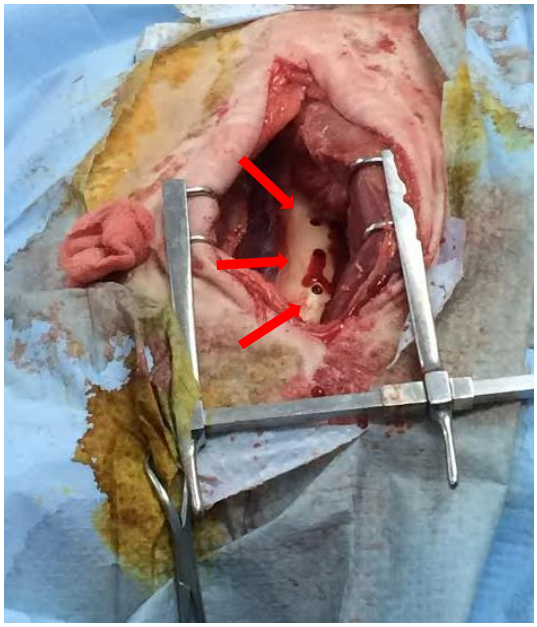

Figure B.1 – 3/5 femur defects to be filled with Bonelike

3 – TISSEL Fibrin Glue was used mixed with Bonelike (1mL/1g) (instead of FLOSEAL, which was proved to be cancerous to some soft tissues due to its high content in calcium). On this process, it is used two syringes: one with fibrogen and other with trombine. The content of each syringe is mixed with Bonelike outside the defect. The polymerization reaction occurs during 30s. It is now ready to fill the defect.

APPENDIX C – PCL pellets reduction to powder for SFM: Optimization Process

Before SFM process, PCL pellets were reduced to powder, increasing the superficial area in order to enhance physical mixture, promoting its interaction with sc-CO2 and reducing the needed processing/contact time. It was observed that a thicker PCL powder was more difficult to mix with SBA-15 silica nanoparticles than a thinner one. The preparation of PCL into powder form was optimized from previous works (Rosa *et al.*, 2013; Churro *et al.*, 2015). In order to so, 12 g of PCL in original pellet form were dissolved into approximately 200mL of acetone under strong magnetic stirring. After complete solubilisation, the solution composed of PCL and acetone was precipitated by anti-solvent precipitation: 20mL of methanol and then 20mL of distilled water (added drop by drop). Then, it was left for sedimentation. PCL was left drying during 2/3 weeks in a ventilated hotte at room temperature. PCL powder was sieved using two test sieves with a width of 0.600mm and 0.250mm (Retshc 5657 Haan w., Germany). The powder was then separated and weighted. In a first stage, the yield of intermediate powder was calculated, because only this size was being used. In a second approach, it was concluded, by macroscopic observation of the processed samples after SFM, that the three sizes of powder could be used simultaneously in order to avoid material waste. Samples were prepared with only one size, or with the three sizes simultaneously in different proportions. For the last, to prepare the composite biomaterials, powder was used proportionality according to the particle size distribution after pellet reduction: 66.7 wt.% of thicker powder (0.600mm < d < 1 mm), 16.65 wt.% of intermediate powder (0.250mm < d < 0.600mm) and 16.65 wt.% of thinner powder (d < 0.250mm). The SFM process is influenced by the particle size since the smaller the powder, higher is the transference area and so shorter is the required processing time. In this work, the samples were processed with a soak/contact time with sc-CO_2 of 2 hours, which is more than enough to guarantee that all the PCL is saturated.

APPENDIX D – Macroscopic analyse of SFM Monoliths

The effect of PCL powder size, GF molar concentration and the addition of SBA-15 silica nanoparticles were evaluated macroscopically. Photographs were taken and can be seen in the next figure.

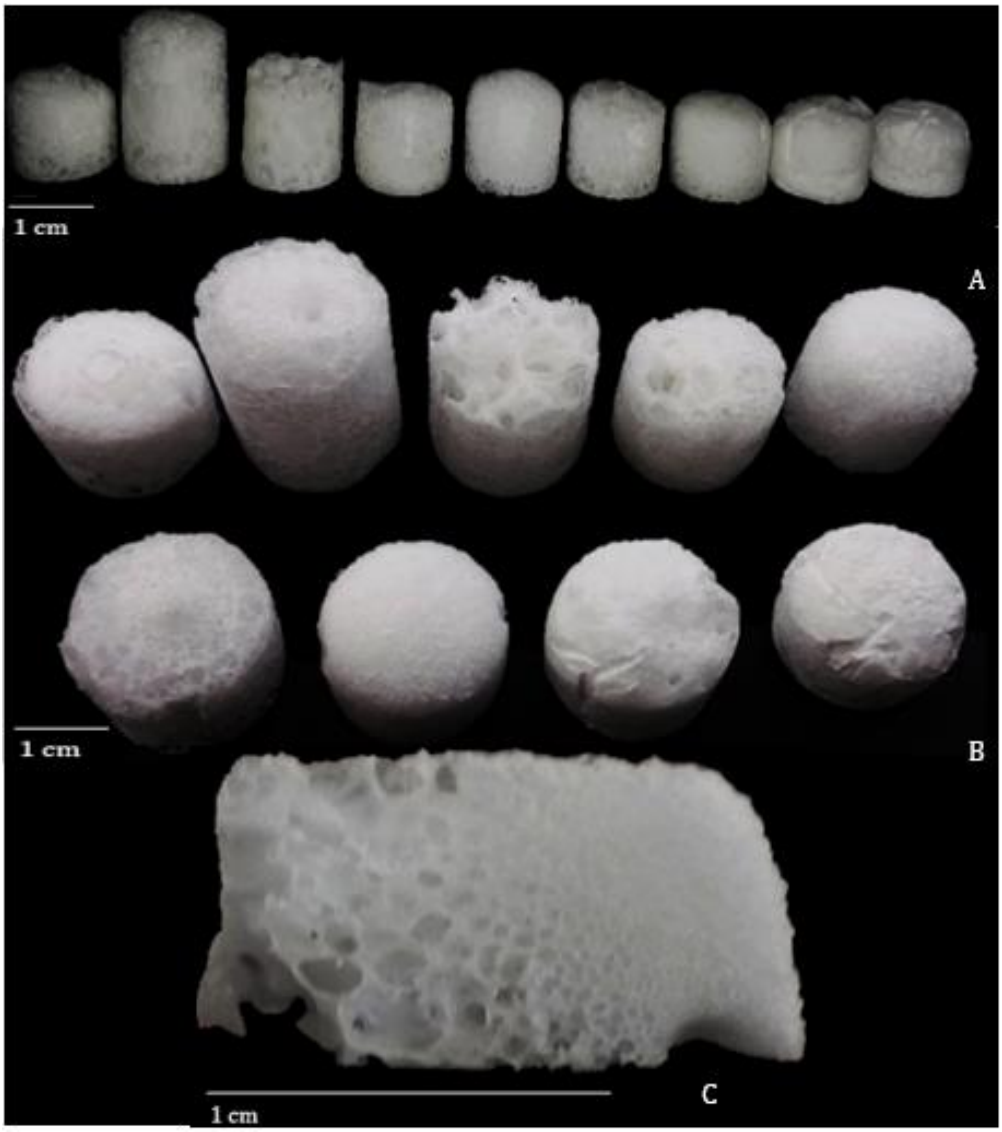

Figure D.1 – Macroscopic visualization of SFM processed samples, side view (A) and top view (B). On A, from left to right: A84, A98, M98, T98, A74, M74, T74, A98+SNPs, A74+SNPs. On B: above, from the left to right: A84, A98, M98, T98, A74. Down, from the left to right: M74, T74, A98+SNPs and A74+SNPs. In C, slice cut top-to-bottom of sample A74+SNPs: PCL 3 sizes + 74 molar % of GF + 17 wt.% SBA-15. The left side corresponds to the bottom and the right side to the top. Scale bar:1 cm.

It is possible to observe their average values of diameter, height (Electronic Outside Micrometer), mass and volume after SFM on the next table.

Table D.1 - Diameter, height, mass and volume of SFM processed monolith samples. The monoliths produced with 8% of SNPs were used on the second stage of this work, in order to be grinded into pieces to future incorporation into composite cements. The volume of the samples was calculated considering the produced biomaterial as being approximately a cylinder.

GF, %	**SFM Biomaterials Based PCL**	**Diameter,** cm	**Height,** cm	**Mass,** g	**Volume,** cm^3
74	**A**	1.69±0.04	1.58±0.21	1.00±0.00	3.58±0.42
	M	1.70±0.04	1.39±0.13	0.99±0.01	3.18±0.09
	T	1.67±0.04	1.41±0.04	1.00±0.02	3.11±0.18
	A+SNPs 17%	1.73±0.04	1.30±0.03	1.16±0.03	3.09±0.08
84	**A**	1.68±0.03	1.86±0.28	1.02±0.02	4.18±0.69
98	**A**	1.75±0.03	2.12±0.33	1.00±0.12	5.12±0.84
	M	1.73±0.03	1.79±0.06	0.99±0.12	4.22±0.01
	T	1.67±0.04	1.60±0.02	1.06±0.03	3.54±0.03
	A+SNPs 17%	1.71±0.04	1.73±0.24	1.29±0.03	4.00±0.47
	A+SNPs 8%	**1.73±0.04**	**1.82±0.15**	**1.31±0.01**	**4.28±0.37**

The last composite monolith (A98 +SNPs 8%) is the optimized one, that will be grinded and sieved into pieces for cement incorporation.

Considering the values of diameters of the composites it is clear that all of them have approximately the same value, since the two used PTFE beakers are geometrically similar. It was expected that the composition of the sample had influence on the value of height and mass. Despite the samples were duplicates two by two, and were processed under the same operating conditions, the values of height are not similar for all pairs, which is an important disadvantage of the SFM process, since there is not an accurate control on the pore size and distribution which directly influences the height of the sample (despite keeping constant biomaterial composition and all the operating conditions). The sample with higher height was the sample A98, produced with the three sizes of PCL and 98 molar concentration of GF, which could be, possibly, caused by the large percentage of thicker PCL powder particles. Generically, the samples produced with all sizes of PCL powders and without silica content have higher height than the samples produced with middle and thinner powder. However, considering the deviation of the samples A74 and A98, it is possible to conclude that the height difference between the different PCL powder size was not significant and it was assumed that the 2 hours of contact with sc-CO_2 were completely sufficient to melt all the PCL powder independently of their size. It is also observed that samples produced with 98 of molar concentration of GF are typically higher than the samples produced with lower amount, since GF is acting as porogenic agent, producing larger pores,

which directly influences the height of the sample. The lowest sample was the A74+SNPs. It is clear that composite samples (with 17 wt. % of silica nanoparticles) are lower than the same formulation produced without silica.

The values obtained for mass of the samples directly depend on their composition so, the samples produced with 17 wt. % of silica nanoparticles are, naturally, heavier than the others, since SNPs bulk density (1.8 $g.cm^{-3}$) is higher than bulk PCL density (1.1 $g.cm^{-3}$). The quantity of GF could also make the samples heavier, however, this effect was not significant with exception to the sample A98 + SNPs, since the maximum used volume of GF was 133μL (GF density=1.09 $g.cm^{-3}$). The values obtained for volume were calculated considering the samples approximately cylinders, and are directly related with the values of heights.

APPENDIX E – SDT: values of some SFM monoliths and pieces

On the next table is possible to see the values of melting and degradation temperatures (ºC) and crystallinity degrees (χ_c, %) for some SFM monoliths.

Table E.1. – SDT results for some SFM-monoliths

SFM processed monolith	Melting temperature,, ºC	Degradation temperature,, ºC	Crystallinity degree,χ_c, %
A74	63.62±5.09	406.83±7.00	86.58±2.56
A74 + SNPs 17%	68.42±4.90	410.66±8.10	51.56±2.57
A84	61.35±4.92	403.73±5.37	43.96±2.45
A98	61.51±5.26	424.00±5.66	54.75±3.68
A98 + SNPs 17%	72.71±5.49	436.24±5.32	56.57±1.43

On the next figure, it is possible to see the measure of the effective percentage of weight of SNPs. It was possible to observe that the average value of the organic mass loss was 92.35%, which consequently leads to a real SBA-15 content of 7.65% for this example.

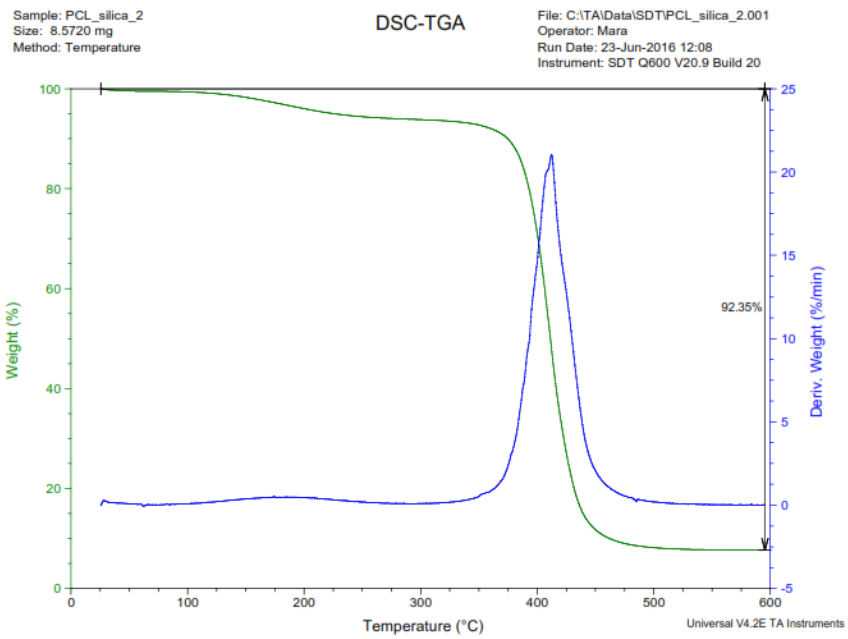

Figure E.1 – SDT of SFM-processed pieces in order to access their real inorganic content

APPENDIX F – Macroscopic results of cement formulations

Table F.1– Liquid to powder ratio (L/P), diameter, mechanical height, mass and volume of composite produced cements. The volume of the samples were calculated considering that the produced cements were approximately cylinders.

Cement Composites	**L/P,** mL/g	**Diameter,** cm	**Mechanical Height,** cm	**Mass,** g	**Volume,** cm^3
G10N6P6	1.07	1.58±0.02	2.38±0.11	1.31±0.18	4.65±0.35
G10N6P12	0.99	1.59±0.01	2.39±0.02	1.85±0.18	4.74±0.05
G10N18P6	0.99	1.47±0.13	2.21±0.15	2.04±1.29	3.75±1.02
G10N18P12	1.03	1.60±0.00	2.40±0.16	1.61±0.06	4.82±0.29
G15N12P9	1.06	1.37±0.02	2.05±0.04	1.41±0.08	3.02±0.06
G20N6P6	1.06	1.47±0.05	2.20±0.23	1.45±0.10	3.73±0.64
G20N6P12	1.03	1.45±0.02	2.17±0.03	1.24±0.14	3.58±0.08
G20N18P6	1	1.42±0.07	2.12±0.01	1.51±0.44	3.36±0.35
G20N18P12	1.04	1.43±0.08	2.15±0.11	1.41±0.34	3.45±0.61

APPENDIX G – Mechanical Analysis: Curve of Stress (MPa) vs Strain (mm/mm)

It is shown on the next figure an example of an obtained curve stress vs strain. It is possible to identify two different zones:

1 - Elastic zone: Strain: 0 to 0.02 mm/mm (almost linear behaviour)

2 - Collapse zone: Strain: from 0.02 mm/mm

-Densification zone was not possible to observe on the assays performed to the cements

These zones are separated by two points:

- Rupture Point - separates elastic zone from collapse zone: Strain ~ 0.02 mm/mm (red arrow).
- Failure Point - separates collapse zone from densification zone: Strain ~ 0.085 mm/mm. Assay was finished when this point was reached (black arrow).

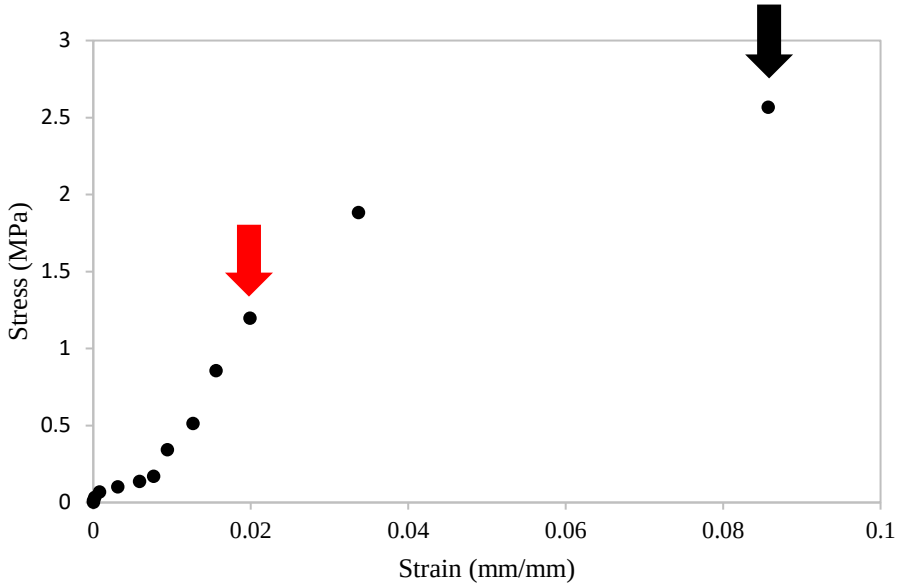

Figure G.1 – Example of a curve Stress (MPa) vs Strain (mm/mm) of the cement composite G20N6P6. The red arrow points to the rupture point. The black arrow points the failure point.